KvS regulatory subunits confer drug resistance to Kv2 channels

Robert G. Stewart[1,3], Matthew James Marquis[1], Sooyeon Jo[3], Michael Ferns[1,2], Jon T. Sack[1,2]

Affiliations:
[1] Department of Physiology and Membrane Biology, University of California Davis
[2] Department of Anesthesiology and Pain Medicine, University of California Davis
[3] Department of Neurobiology, Harvard Medical School

Corresponding author email: jsack@ucdavis.edu

Conflict of interest statement: The authors declare no conflicts of interest.

Acknowledgments:

We thank the human tissue donors and their families for their generous donations. We thank Sierra Donor Services for recovering human dorsal root ganglia, as well as Sean Van Slyck and Marnae Salampessy, and Theanne Griffith for helping arrange for human tissue. We thank Bryan Copits, Ted Price, and Juliet Mwirigi for advice on culturing human neurons. We thank Cyrrus Espino, Hai Nguyen, and Geir Hareland for preparation of human tissues. This research was supported the University of California Davis and U.S. National Institutes of Health grant R03TR004200.

ABSTRACT

KvS proteins are pore-forming voltage-gated potassium channel subunits that must co-assemble into heterotetramers with Kv2.1 (*KCNB1*) or Kv2.2 (*KCNB2*) subunits to form functional channels. In mammals, KvS subunits encompass the Kv5.1 (*KCNF1*), Kv6.1 (*KCNG1*), Kv6.2 (*KCNG2*), Kv6.3 (*KCNG3*), Kv6.4 (*KCNG4*), Kv8.1 (*KCNV1*), Kv8.2 (*KCNV2*), Kv9.1 (*KCNS1*), Kv9.2 (*KCNS2*), and Kv9.3 (*KCNS3*) proteins. While Kv2 proteins are broadly expressed in electrically excitable cells, KvS mRNAs are enriched in unique subsets of these cells. The physiological functions of KvS-containing channels are poorly understood and no drugs are known to selectively modulate KvS subunits. Here, we identify a pair of potent Kv2-selective inhibitors which distinguish conductances of KvS-containing channels. We find that conductances of KvS-containing channels are resistant to the pore-blocker RY785 yet remain sensitive to the voltage sensor modulator guangxitoxin-1E (GxTX). We show that this pattern of inhibitor sensitivities is consistent among subunits from Kv5, Kv6, Kv8, and Kv9 families. By deploying these inhibitors we find that mouse superior cervical ganglion neurons have conductances consistent with Kv2, but not KvS-containing channels. In contrast, mouse and human dorsal root ganglion neurons have conductances consistent with KvS/Kv2 heteromeric channels. These results provide an approach to pharmacologically distinguish KvS-containing from Kv2-only channels, and identify endogenous KvS conductances.

INTRODUCTION

Proteins of the Kv2 family (Kv2.1 and Kv2.2) are voltage-gated K^+ channel subunits that assemble into tetramers to form channels that selectively conduct potassium ions across cell membranes (Kihira et al., 2010; Fernández-Mariño et al., 2023). Kv2 subunits are broadly expressed in electrically excitable cells throughout the body and have important ion-conducting and non-conducting functions (Liu and Bean, 2014; Bishop et al., 2015; Kirmiz et al., 2018; Vierra et al., 2021; Matsumoto et al., 2023). Electrically, Kv2 proteins are voltage-activated channels that regulate excitability of cell membranes (Guan et al., 2007; Liu and Bean, 2014; Speca et al., 2014; Zheng et al., 2019).

A potential source of diversity for channels containing Kv2 subunits comes from ten proteins of the mammalian voltage-gated K^+ channel superfamily that have been classified as "regulatory" (Kobertz, 2018) or "silent" (Bocksteins et al., 2009) subunits. Here, we refer to these proteins collectively as KvS subunits. The KvS proteins (Kv5.1, Kv6.1-6.4, Kv8.1-8.2, and Kv9.1-9.3) have sequence similarity to pore forming Kv2 subunits. However, KvS subunits have not been found to form functional channels as homomers. Rather, KvS subunits co-assemble with Kv2 subunits to form heteromeric channels (Salinas et al., 1997a; Kramer et al., 1998). Each KvS-containing channel has biophysical properties distinct from Kv2 channels (Post et al., 1996; Salinas et al., 1997b; Kramer et al., 1998; Richardson and Kaczmarek, 2000; Zhong et al., 2010; Bocksteins et al., 2012; Bocksteins et al., 2017). Studies of Kv2 and KvS stoichiometries have found evidence for predominance of 2:2 (Moller et al., 2020) or 3:1 Kv2:KvS (Kerschensteiner et al., 2005; Pisupati et al., 2018). KvS mRNAs are expressed in tissue and cell-specific manners that overlap with Kv2.1 or Kv2.2 expression (Castellano et al., 1997; Salinas et al., 1997b; Kramer et al., 1998; Bocksteins et al., 2012; Bocksteins and Snyders, 2012; Bocksteins, 2016). These findings suggest that KvS subunits could generate extensive endogenous diversity of heteromeric KvS/Kv2 channels, between and within cells. Consistent with this, genetic mutations and gene-targeting studies have linked disruptions in the function of KvS subunits to epilepsy (Jorge et al., 2011), neuropathic pain sensitivity (Tsantoulas et al., 2018), labor pain (Lee et al., 2020), male infertility (Regnier et al., 2017), and retinal cone dystrophy (Wu et al., 2006; Hart et al., 2019; Inamdar et al., 2022). However, a lack of KvS-specific research tools has limited functional studies of KvS proteins.

No drugs are known to be selective for KvS proteins. Heteromeric channels with both KvS and Kv2 subunits do, however, have some distinct pharmacology from channels that contain only Kv2 subunits. Quaternary ammonium compounds, 4-aminopyridine, and other broad-spectrum K^+ channel blockers have different potencies against certain KvS-containing channels as compared to Kv2 channels (Post et al., 1996; Thorneloe and Nelson, 2003; Stas et al., 2015). However, due to the promiscuity of these blockers, they cannot categorically identify endogenous KvS conductances.

Two categories of highly-selective Kv2 channel inhibitors have been identified. One class is inhibitory cystine knot peptides from spiders. The tarantula toxin Guangxitoxin-1E (GxTX) has remarkable specificity for Kv2 channel subunits over other voltage gated-channels (Herrington et al., 2006; Thapa et al., 2021). GxTX binds to the voltage sensor of each Kv2 subunit (Milescu et al., 2009), and stabilizes that voltage sensor in a resting state to prevent channel opening (Tilley et al., 2019). GxTX binding requires a specific sequence of residues, TIFLTES, at the extracellular end of the S3 transmembrane helix (Milescu et al., 2013). This GxTX-binding sequence is conserved between the Kv2 channels, but is not retained by any KvS subunit. A second class of selective Kv2 inhibitors is a family of small molecules discovered in a high throughput screen for use-dependent Kv2 inhibitors (Herrington et al., 2011). Of these, RY785 is the most selective for Kv2 channels over other channel types. RY785 acts like a pore blocker and likely binds in the central cavity of Kv2.1 channels (Marquis and Sack, 2022). We recently found that coexpression of Kv5.1 with Kv2.1 led to a conductance that was resistant to RY785 (Ferns et al., 2024).

In this study, we identify that a pair of potent, Kv2-selective inhibitors, GxTX and RY785, can distinguish conductances of Kv2 homomers from heteromers containing KvS subunits from the Kv5, Kv6, Kv8, and Kv9 subfamilies. We then deploy this pharmacology to identify endogenous KvS-like conductances in somatosensory neurons.

METHODS

- Mice

Studies were approved by the UC Davis and Harvard Medical School Institutional Animal Care and Use Committee and conforms to guidelines established by the NIH. Mice were maintained on a 12 hr light/dark cycle, and food and water were provided ad libitum. The *Mrgprd*^{GFP} mouse line was a generous gift from David Ginty (Harvard University, Boston MA) (MGI: 3521853).

- Human tissue collection

Human DRG were obtained from Sierra Donor Services. The donor was a 58-year-old Asian Indian female and DRG were from the 1st and 2nd lumbar region (cause of death: Stroke). DRG were extracted 6 hours after aortic cross clamp and placed in an ice cold NMDG-aCSF solution containing in mM: 93 NMDG, 2.5 KCl 1.25 NaH2PO4, 30 NaHCO3, 20 HEPES, 25 Glucose, 5 L-Ascorbic acid, 2 Thiourea, 3 Na pyruvate, 10 MgSO4 and 0.5 CaCl2 pH adjusted to 7.4 with NMDG. Human DRG were obtained from the organ donor with full legal consent for use of tissue for research in compliance with procedures approved by Sierra Donor Services.

- CHO cell culture and transfection

The CHO-K1 cell line transfected with a tetracycline-inducible rat Kv2.1 construct (Kv2.1-CHO; Trapani and Korn, 2003) was cultured as described previously (Tilley et al., 2014). Transfections were achieved with Lipofectamine 3000 (cat. #; Life Technologies). 1 µl Lipofectamine was diluted, mixed, and incubated in 25 µl of Opti-MEM (product no. 31985062, lot no. 1917064; Gibco-BRL). Concurrently, 0.5 µg of KvS or AMIGO1 or Navβ2, 0.5 µg of pEGFP, 2 µl of P3000 reagent and 25 µl of Opti-MEM were mixed. DNA and Lipofectamine 3000 mixtures were mixed and left at room temperature for 15 min. This transfection cocktail mixture was added to 1 ml of culture media in a 24 well cell culture dish containing Kv2.1-CHO cells and incubated at 37°C in 5% CO_2 for 6 h before the media was replaced. Immediately after media was replaced, Kv2.1 expression was induced in Kv2.1-CHO cells with 1 µg/ml minocycline (cat. #ALX-380-109-M050; Enzo Life Sciences), prepared in 70% ethanol at 2 mg/ml. Voltage clamp recordings were performed 12-24 hours later. During recordings, the experimenter was blinded to which cells had been transfected with KvS, or Navβ2 or AMIGO1. Human Kv5.1, human Kv6.4 and human Kv8.1, AMIGO1-YFP, and pEGFP plasmid plasmids were gifts from James Trimmer (University of California, Davis, Davis, CA). Human Kv9.1, human Kv9.3 plasmids were purchased from addgene. Navβ2 plasmid was a gift from Al George (Northwestern University).

- Neuron cell culture

  - Mouse

Cervical, thoracic and lumbar DRGs were harvested from 7- to 10-week-old *Mrgprd*^{GFP} mice and transferred to Hank's buffered saline solution (HBSS) (Invitrogen). Ganglia were treated with collagenase

(2 mg/ml; Type P, Sigma-Aldrich) in HBSS for 15 min at 37°C followed by 0.05% Trypsin-EDTA (Gibco) for 2.5 min with gentle rotation. Trypsin was neutralized with culture media (MEM, with l-glutamine, Phenol Red, without sodium pyruvate) supplemented with 10% horse serum (heat-inactivated; Gibco), 10 U/ml penicillin, 10 µg/ml streptomycin, MEM vitamin solution (Gibco), and B-27 supplement (Gibco). Serum-containing media was decanted and cells were triturated using a fire-polished Pasteur pipette in MEM culture media containing the supplements listed above. Cells were plated on laminin-treated (0.05 mg/ml, Sigma-Aldrich) 5 mm German glass coverslips (Bellco Glass, 1943-00005), which had previously been washed in 70% ethanol and sterilized with ultraviolet light. Cells were then incubated at 37°C in 5% CO_2. Cells were used for electrophysiological experiments 24–38 hr after plating.

SCGs were harvested from Swiss Webster (CFW) mice (postnatal day 13-15, either sex) and treated for 20 min at RT with 20 U/ml papain (Worthington Biochemical, Lakewood, NJ), 5 mM dl-cysteine, 1.25 mM EDTA, and 67 µM β-mercaptoethanol in a Ca^{2+}, Mg^{2+}-free (CMF) Hank's solution (Gibco, Grand Island, NY) supplemented with 1 mM Sodium Pyruvate (Sigma-Aldrich, St. Louis, MO), and 5 mM HEPES (Sigma-Aldrich, St. Louis, MO). Ganglia were then treated for 20 min at 37°C with 3 mg/ml collagenase (type I; Roche Diagnostics) and 3 mg/ml dispase II (Roche Diagnostics) in CMF Hank's solution. Cells were dispersed by titration with fire-polished Pasteur pipettes in a solution composed of two media combined in a 1:1 ratio: Leibovitz's L-15 (Invitrogen, Grand Island, NY) supplemented with 5 mM HEPES, and DMEM/F12 medium (Invitrogen). Cells were then plated on glass coverslips and incubated at 37°C (95% O_2, 5% CO_2) for 1 h, after which Neurobasal medium (Invitrogen) with B-27 supplement (Invitrogen), penicillin and streptomycin (Sigma) was added to the dish. Cells were incubated at 25°C (95% O_2, 5% CO_2) and used within 10 h.

- Human

Dura were removed from human DRG with a scalpel in ice cold NMDG-aCSF solution (Valtcheva et al., 2016). Human DRG were then cut into approximately 1 mm thick sections and were placed in 1.7 mg/mL Stemxyme (Worthington Biochemical, LS004107) and 6.7 mg/mL DNAse I (Worthington Biochemical, LSOO2139) diluted in HBSS (Thermo Fisher Scientific, 14170161) for 12 hours at 37°C. DRG were then triturated with a fire-polished Pasteur pipette and passed through a 100 µm cell strainer. Cells were then spun at 900 g through 10% BSA. The supernatant was removed, and cells were resuspended in human DRG culturing media that contained 1% penicillin/streptomycin, 1% GlutaMAX (Gibco, 35050-061), 2% NeuroCult SM1 (05711, Stemcell technologies), 1% N2 Supplement (Thermo Scientific, 17502048), 2% FBS (Gibco, 26140-079) diluted in BrainPhys media (Stemcell tehnologies, 05790). DRG neurons were plated on poly-D lysine treated (0.01 mg/mL) 5 mm German glass coverslips, which had previously been washed in 70% ethanol and sterilized with ultraviolet light. DRG neurons were then incubated at 37°C in 5% CO_2. Human DRG neuron experiments were performed up to 7 days after plating.

- Whole cell voltage clamp of CHO cells

Voltage clamp was achieved with a dPatch amplifier (Sutter Instruments) run by Sutterpatch (Sutter Instruments). Solutions for Kv2.1-CHO cell voltage-clamp recordings: CHO-internal (in mM) 120 K-methylsulfonate, 10 KCl, 10 NaCl, 5 EGTA, 0.5 $CaCl_2$, 10 HEPES, 2.5 MgATP pH adjusted to 7.2 with KOH, 289 mOsm. CHO-external (in mM) 145 NaCl, 5 KCl, 2 $CaCl_2$, 2 $MgCl_2$, 10 HEPES pH adjusted to 7.3 with NaOH, 298 mOsm. Osmolality was measured with a vapor pressure osmometer (Wescor, 5520). The calculated liquid junction potential for the internal and external recording solutions was 9.7 mV and was not accounted for. For voltage-clamp recordings, Kv2.1-CHO cells were detached in a PBS-EDTA solution (15040-066, Gibco), spun at 500 g for 2 minutes and then resuspended in 50% cell culture media and

50% CHO-external recording solution. Cells were then added to a recording chamber (Warner Cat#64–0381) and were rinsed with the CHO-external patching solution after adhering to the bottom of the recording chamber. Transfected Kv2.1-CHO cells were identified by GFP fluorescence and were selected for whole cell voltage clamp. Thin-wall borosilicate glass recording pipettes (BF150-110-10, Sutter) were pulled with blunt tips, coated with silicone elastomer (Sylgard 184, Dow Corning), heat cured, and tip fire-polished to resistances less than 4 MΩ. Series resistance of 2–14 MΩ was estimated from the whole-cell parameters circuit. Series resistance compensation between 13 and 90% was used to constrain voltage error to less than 15 mV, lag was 6 µs for most experiments or 100 µs for concentration-effect experiments. Capacitance and Ohmic leak were subtracted using a P/4 protocol. Output was low-pass filtered at 5 kHz using the amplifier's built-in Bessel and digitized at 25 kHz or, for concentration-effect experiments, 1 and 10 kHz. Experiments were performed on Kv2.1-CHO cells with membrane resistance greater than 1 GΩ assessed prior to running voltage clamp protocols while cells were held at a membrane potential of –80 mV. Stocks of RY785 (gift from Bruce Bean, Harvard or Cayman, 19813) in DMSO were 1 mM for dilutions to 1 µM or 35 mM for concentration-effect experiments. Stocks of GxTX-1E Met35Nle (Tilley et al., 2014) in water were 10 µM. Stocks were stored frozen and diluted in recording solution just prior to application to cells.. Solutions were flushed over cells at a rate of approximately 1 mL/min. Concentrated RY785 and GxTX stocks were stored at -20 °C. Kv2.1-CHO cells were given voltage steps from -80 mV to 0 mV for 200 ms every 6 seconds during application of RY785 until currents stabilized. When vehicle control was applied to cells, 0 mV steps were given for a similar duration. The DMSO concentration in RY785 and vehicle control solutions was 0.1%. Perfusion lines were cleaned with 70% ethanol then doubly-deionized water. For concentration-effect experiments, changes in current amplitude due to solution exchange were controlled for by treating every other tested cell with multiple washes of the same, 0.35 µM RY785 solution instead of increasing concentrations of RY785. The timing of these control washes was similar to that of the washes in concentration-effect experiments.

- Whole cell voltage clamp of mouse and human dorsal root ganglion neurons

Whole cell recordings from mouse and human neurons were performed using the same methods as CHO cell recordings with the following exceptions. Voltage clamp was achieved with a dPatch amplifier run by SutterPatch or an AxoPatch 200B amplifier (Molecular Devices) controlled by PatchMaster software (v2x91, HEKA Elektronik) via an ITC-18 A/D board (HEKA Instruments Inc). Solutions for voltage-clamp recordings: internal (in mM) 140 KCl, 13.5 NaCl, 1.8 $MgCl_2$ 0.09 EGTA, 4 MgATP, 0.3 Na_2GTP, 9 HEPES pH adjusted to 7.2 with KOH, 326 mOsm. The external solution contained (in mM) 3.5 KCl, 155 NaCl, 1 $MgCl_2$, 1.5 $CaCl_2$, and 0.01 $CdCl_2$, 10 HEPES 10 glucose pH adjusted to 7.4 with NaOH, 325 mOsm. The calculated liquid junction potential for the internal and external recording solutions was 4.14 mV and was not accounted for. For voltage-clamp recordings, neurons on cover slips were placed in the same recording chamber used for CHO cell recordings and were rinsed with an external patching solution. Neurons from *Mrgprd*^{GFP} mice with green fluorescence were selected for recordings. Human DRG neurons with cell capacitances between 22.5 and 60 pF were used. After whole-cell voltage clamp was established, the external solution was exchanged with external solution containing 100 nM alpha-dendrotoxin (Alomone), 1 µM TTX, 3 µM AmmTX3 (Alomone), 100 µM 4-aminopyridine, and 10 µM A-803467 (Tocris). After addition of 1 µM RY785 neurons were given 10 steps to -20 mV for 500 ms to allow for voltage dependent block of RY785. Thin-wall borosilicate glass recording pipettes were pulled with blunt tips, coated with silicone elastomer, heat cured, and tip fire-polished to resistances less than 2 MΩ. Series resistance of 1–4 MΩ was estimated from the whole-cell parameters circuit. Series

resistance compensation between 55 and 98% was used to constrain voltage error to less than 15 mV. Ohmic leak was not subtracted. Neurons were held at a membrane potential of –70 mV.

- Whole cell voltage clamp of mouse superior cervical ganglion neurons

Whole cell recordings from mouse superior cervical ganglion neurons were performed using the same methods as dorsal root ganglion recordings with the following exceptions. Recordings were performed using an Axon Instruments Multiclamp 700B Amplifier (Molecular Devices). Voltage or current commands were delivered and signals were recorded using a Digidata 1321A data acquisition system (Molecular Devices) controlled by pCLAMP 9.2 software (Molecular Devices). Solutions for voltage-clamp recordings: internal (in mM) 155 K-Aspartate, 15 NaCl, 1.8 MgCl2, 0.1 EGTA, 10 HEPES pH adjusted to 7.2 with KOH, 312 mOsm. The calculated liquid junction potential for the internal and external recording solutions was -10 mV and was not accounted for. After establishing whole-cell recording, cell capacitance was nulled and series resistance was partially (60%) compensated to constrain voltage error to less than 2 mV. The cell was then lifted and placed in front of a series of quartz fiber flow pipes for rapid solution exchange and application of RY785 and GxTX. Electrodes were pulled on a Sutter P-97 puller (Sutter Instruments) and shanks were wrapped with Parafilm (American National Can Company) to allow optimal series resistance compensation without oscillation.

- Ionic current analysis

Activation kinetics were fit from 10-90% of current rise with the power of an exponential function:

Equation 1

$$I_K = A\left(1 - e^{\frac{-t}{\tau_{act}}}\right)^{\sigma}$$

Fit such that (time) t = 0 is the beginning of a voltage step from the holding potential. The t = 0 mark was adjusted to 100 μs after voltage step start to correct for filter delay and cell charging. A = maximum current amplitude, τ_{act} = time constant of activation and σ = sigmoidicity.

Conductance values were determined from tail current levels at 0 mV after 200 ms steps to the indicated voltage. Tail currents were mean current amplitude from 1 to 5 ms into the 0 mV step. Conductance voltage relations were fit with the Boltzmann function:

Equation 2

$$f(V) = A\left(1 + e^{-\left(\left(V - V_{\frac{1}{2}}\right)\frac{zF}{RT}\right)}\right)^{-1}$$

Where V = voltage, A = the amplitude, z = number of elementary charges, F = Faraday's constant, R = the universal gas constant, and T = temperature (held at 295° K).

Deactivation kinetics were fit with a double exponential:

Equation 3

$$f(x) = y_0 + A_1 e^{\frac{-(x-x_0)}{\tau_1}} + A_2 e^{\frac{-(x-x_0)}{\tau_2}}$$

Where x = time, y_0 = the initial current amplitude, x_0 = the start time of the exponential decay, τ_1 = first component time constant, A_1 = first component current amplitude, τ_2 = second component time constant, A_2 = second component current amplitude

- Multiplex in situ hybridization

A 6-week-old *Mrgprd*^{GFP} mouse was briefly anesthetized with 3–5% isoflurane and then decapitated. The spinal column was dissected, and the left and right L1 DRG were removed and drop fixed for 12 minutes in ice cold 4% paraformaldehyde in 0.1 M phosphate buffer (PB) pH adjusted to 7.4. The L1 vertebrae was identified by the 13th rib. The DRG was washed 3× for 10 min each in PB and cryoprotected at 4°C in 30% sucrose diluted in PB for 2 hr. The DRG were then frozen in Optimal Cutting Temperature (OCT) compound (Fisher, 4585) and stored at –80°C until sectioning. Samples were cut into 20 µm sections on a freezing stage sliding microtome and were collected on Colorfrost Plus microscope slides (Fisher Scientific, 12-550-19). Sections were processed for RNA *in situ* detection using an RNAscope Fluorescent Detection Kit according to the manufacturer's instructions (Advanced Cell Diagnostics) and the following probes: *KCNF1* (508731, mouse) or *KCNS1* (525941, mouse). TSA Vivid 650 Fluorophore was used to label probes (TSA Vivid, 7527) Following in situ hybridization, immunohistochemistry to label GFP was performed. Sections were incubated in vehicle solution (4% milk, 0.2% triton diluted in PB) for 1 hr at room temperature (RT). Tissue was then incubated in a rabbit polyclonal anti-GFP antibody (Rockland 600-401-215S) diluted 1:1000 in vehicle overnight at 4°C. Sections were washed three times in vehicle for 5 minutes per wash and then incubated in a goat anti-rabbit secondary antibody (Invitrogen, A-11008) diluted 1:1500 in vehicle. Sections were then mounted with Prolong Gold (Thermo Fisher, P36930) and #1.5 cover glass (Fisher Scientific, NC1776158).

- Imaging

Images were acquired with an inverted scanning confocal and airy disk imaging system (Zeiss LSM 880 Airyscan, 410900-247-075) run by ZEN black v2.1. Laser lines were 488 nm and 633 nm. Images were acquired with a 0.8 NA 20x objective (Zeiss 420650-9901) details in figure legends.

- Statistics

All statistical tests were performed in Igor Pro software version 8 (Wavemetrics, Lake Oswego, OR). Independent replicates (n) are individual cells/neurons while biological replicates (N) are individual mice. Details of statistical tests are in the figure legends.

RESULTS

- Kv2.1/Kv8.1 heteromers are resistant to RY785 but sensitive to GxTX

To test whether Kv2 inhibitors also inhibit KvS channels, we transfected KvS cDNA in a stable cell line that could be induced to express Kv2.1 (Kv2.1-CHO) and recorded whole cell currents. We previously found that 1 µM RY785 or 100 nM GxTX blocked the voltage-gated K^+ conductance of this Kv2.1-CHO cell line leaving 1 ± 2% (SEM) or 0 ± 0.1% (SEM) current remaining respectively at 0 mV (Tilley et al., 2019; Marquis and Sack, 2022). Recently we found that transfection of Kv5.1 into these Kv2.1-CHO cells could create a conductance which was not blocked by 1 µM RY785 (Ferns et al., 2024). Like Kv5.1, we find that after transfection of Kv8.1 into Kv2.1-CHO cells, a component of the delayed rectifier current became resistant to 1 µM RY785 (Fig 1 A). This RY785-resistant current was however inhibited by 100 nM GxTX, suggesting that the GxTX-sensitivity arises from inclusion of Kv2.1 subunits in the channels underlying the RY785-resistant current. We propose that the RY785-resistant yet GxTX-sensitive currents we observed were carried by Kv8.1/2.1 heteromeric channels. The fraction of RY785-resistant current had pronounced cell-to-cell variability (Fig 1 D). Co-expression of KvS subunits can result in Kv2 homomers and KvS/Kv2 heteromers (Pisupati et al., 2018), and we suspect the variability in the RY785-sensitive fraction is due to cell-to-cell variability in the proportion of Kv8.1-containing channels.

As a control, we transfected Kv2.1-CHO cells with a protein not expected to interact with Kv2.1 (Navβ2). In Kv2.1-CHO cells transfected with Navβ2, 1 µM RY785 blocked Kv2.1 conductances leaving 4 ± 0.6 % (mean ± SEM) of current (Fig 1 B and D). We also transfected Kv2.1-CHO cells with a member of the AMIGO family of Kv2-regulating transmembrane proteins. AMIGO1 promotes voltage sensor activation of Kv2.1 channels in these Kv2.1-CHO cells (Sepela et al., 2022). 1 µM RY785 blocked Kv2.1 conductances in cells transfected with AMIGO1, leaving 0.6 ± 1% (SEM) of current (Fig 1 C and D). These controls indicate that transfection of a set of other transmembrane proteins did not confer resistance to RY785, suggesting that the RY785 resistance is not induced by overexpression of non-KvS transmembrane proteins.

To determine whether the resistance to RY785 provided by Kv8.1 was absolute, we performed an RY785 concentration-effect experiment. To pre-block Kv2.1 homomers we began concentration-effect measurements at 0.35 µM RY785, which we expect to block 98% of homomers based on our estimated K_D of 6 nM RY785 for the Kv2.1 currents in these Kv2.1-CHO cells (Marquis and Sack, 2022). Currents resistant to 0.35 µM RY785 were blocked by higher concentrations of RY785, with nearly complete block observed in 35 µM RY785 (Fig 2 A). We quantified block of tail currents at 0 mV following a 200 ms step to +80 mV, and normalized to 0.35 µM RY785. This protocol revealed an IC_{50} of 5.1 ± 1.0 µM (SD) (Fig 2 B). The Hill coefficient of 1.2 ± 0.2 is consistent with a homogenous population of RY785-inhibited channels. We had noted that solution exchanges can change current amplitudes and also included interleaved, time-matched solution exchange controls. These controls revealed variable current rundown, approximately 30% on average (Fig 2 C). Following block by 35 µM RY785, washing with 0.35 µM RY785 caused increases in current amplitudes in every trial (Fig 2 D). The run-down and incomplete wash-out indicate that the 5 µM IC_{50} of RY785 for these resistant channels may be an underestimate. Overall, we conclude that Kv8.1-containing channels in these Kv2.1-CHO cells form a pharmacologically homogenous population with an affinity for RY785 ~3 orders of magnitude weaker than for Kv2.1 homomers. Our estimates of the affinities of Kv2.1 homomeric and Kv8.1/Kv2.1 heteromeric channels for RY785 suggest that ~1 µM RY785 elicits nearly complete block of Kv2.1 homomer conductance while blocking little KvS conductance.

- RY785-resistant current is consistent with Kv2.1/Kv8.1.

We wondered whether RY785 block of Kv2 homomers could better reveal the gating of heteromers. While concentrations of RY785 that partially block Kv8.1/Kv2.1 modified the kinetics of voltage-dependent gating, suggesting state-dependent block (Fig 3), we did not observe kinetic differences with 3.5 µM or lower concentrations of RY785. To study the biophysical properties of the Kv8.1 conductance in the Kv2.1-CHO cells, we analyzed currents in 1 µM RY785 to block Kv2 homomers. For comparison, Kv2.1-CHO cells were transfected with a control plasmid and treated with a vehicle control (Fig 4 Supplement 1). We stepped cells to 0 mV from a holding potential of -80 mV and fit current activation with an exponential function (equation 1). Cells transfected with Kv8.1 had a significantly slower time constant of activation as well as a shorter relative activation delay relative to Kv2.1 (Fig 4 A-C, $p < 0.001$ and $p < 0.001$ respectively). Conductance-voltage relations were fit with a Boltzmann function (equation 2) revealing that the half-maximal conductance of Kv8.1-transfected cells is shifted positive relative to Kv2.1 alone (Fig 4 D and E, $p = 0.006$). We did not detect a significant difference in the steepness (z) of the conductance voltage relation (Fig 4 F). Currents from Kv8.1-transfected cells inactivated less after a 10 s step to 0 mV (Fig 4 G and H, $p = 0.002$). The steady-state inactivation of Kv8.1-transfected cells was shifted to more negative voltages and is less steep (Fig 4 I-K, $p = 0.01$ and $p= 0.001$ respectively). These biophysical properties are consistent with a previous report which identifies that co-expression of Kv8.1 with Kv2.1 in *Xenopus* oocytes slows the rate of activation, reduces inactivation and shifts steady-state inactivation to more negative voltages (Salinas et al., 1997b). This previous report also identifies a positive shift in the conductance-voltage relation when Kv8.1 is co-expressed with a Kv2 subunit (Kv2.2), similar to our findings with Kv8.1/Kv2.1. Together these results identify that RY785-resistant currents in cells transfected with Kv8.1 are distinct from Kv2.1 and consistent with the prior reports of Kv8.1/Kv2 biophysics. This validates using RY785 block of Kv2 homomers as a method to reveal the biophysics of a homogenous Kv8.1-containing population.

- A subunit from each KvS family is resistant to RY785 but sensitive to GxTX.

To test if RY785 resistance is a property shared broadly by KvS subunits, we studied a subunit from each KvS subfamily. We had previously found that the sole Kv5 subunit, Kv5.1, was resistant to RY785 (Ferns et al., 2024). We additionally transfected a Kv6 subunit, Kv6.4, and a Kv9 subunit, Kv9.3, to find if they also produced delayed rectifier current resistant to 1 µM RY785 yet sensitive to 100 nM GxTX (Fig 5 A-C). We observed that in 1 µM RY785, >10% of the voltage gated current remained in 12/13 Kv5.1, 9/14 Kv6.4, and 5/5 Kv9.3 transfected cells (Fig 5 D). Like Kv8.1, the fraction of RY785-resistant current had pronounced cell-to-cell variability (Fig 5 D) suggesting the RY785-sensitive fraction could be due to different ratios of functional Kv2.1 homomers to Kv2.1/KvS heteromers. Addition of 100 nM GxTX blocked RY785-resistant current from cells transfected with each of these KvS subunits. A slightly higher fraction of Kv9.3 current remained in 100 nM GxTX, possibly due to Kv9.3 shifting the conductance voltage relationship to more negative voltages (Kerschensteiner and Stocker, 1999). These results show that voltage-gated outward currents in cells transfected with members from each KvS family have decreased sensitivity to RY785 but remain sensitive to GxTX. While we did not test every KvS regulatory subunit, these results suggest that all KvS subunits may provide resistance to 1 µM RY785 yet remain sensitive to GxTX. If RY785 resistance is a general feature of KvS/Kv2 heteromers, then RY785 resistance could be a hallmark of KvS-containing channels.

- The Kv2 conductances of mouse superior cervical ganglion neurons do not have KvS-like pharmacology.

We set out to assess whether RY785 coupled with GxTX could be a means of isolating endogenous Kv2 from KvS-containing channels. We first designed experiments to test whether RY785 could inhibit endogenous Kv2 currents in mice, by studying neurons unlikely to express KvS subunits. Rat superior cervical ganglion (SCG) neurons have robust GxTX-sensitive conductances (Liu and Bean, 2014) yet have little to no KvS transcripts (Sapio et al., 2020). We investigated whether SCG neurons have KvS-like conductances by performing whole cell voltage clamp on dissociated mouse neurons. To help isolate Kv2/KvS currents, we bathed SCG neurons in a cocktail of Nav, Kv1, Kv3, and Kv4 inhibitors and recorded voltage-gated currents. We found that washing neurons with 1 µM RY785 inhibited the majority of current in all SCG neurons, and subsequent washing with 100 nM GxTX and 1 µM RY785 inhibited little if any additional current (Fig 6 A and B). We analyzed tail currents to quantify inhibition, as a hallmark of Kv2 is relatively slow deactivation (Thorneloe and Nelson, 2003; Zheng et al., 2019). Tail currents after application of 1 µM RY785 were significantly decreased by 88 $\pm$ 5 % (mean $\pm$ SEM) in SCG neurons (Fig 6 B, n = 7 neurons, N = 3 mice $p < 0.001$). Subsequent application of 100 nM GxTX did not significantly decrease tail currents (n = 4 neurons, N = 3 mice, $p = 0.06$). To determine if the RY785-sensitive conductances are consistent with previous reports of Kv2 channels, we examined the biophysical properties of the Kv2-like (RY785-sensitive) currents defined by subtraction (Fig 6 C). Channel conductances began at -30 mV and had a half maximal conductance of 4 mV (Fig 6 D). We found that the rate of deactivation of RY785 sensitive currents in SCG neurons is 16 ms $\pm$ 0.6 (mean $\pm$ SEM) at -30 mV (Fig 6 E). These results are consistent with the biophysical properties of Kv2 channels (Kramer et al., 1998; Liu and Bean, 2014; Tilley et al., 2019; Sepela et al., 2022). Of the total conductance sensitive to RY785 and GxTX, 91 $\pm$ 4 % (mean $\pm$ SEM) was sensitive to RY785 (Kv2-like) whereas only 9 $\pm$ 4 % (mean $\pm$ SEM) appeared resistant to RY785 but sensitive to GxTX (KvS-like) (Fig 6 F). Together these results show that 1 µM RY785 was effective at inhibiting the endogenous Kv2 current in these mouse neurons, consistent with Kv2 channels devoid of KvS subunits.

- Mouse nociceptors have KvS-like conductances.

To determine if the RY785/GxTX pharmacology could reveal endogenous KvS channels, we next studied neurons likely to express KvS subunits. Mouse dorsal root ganglion (DRG) somatosensory neurons express Kv2 proteins (Stewart et al., 2024), have GxTX-sensitive conductances (Zheng et al., 2019), and express a variety of KvS transcripts (Bocksteins et al., 2009; Zheng et al., 2019). To record from a consistent subpopulation of mouse somatosensory neurons, we used a *Mrgprd*^{GFP} transgenic mouse line which expresses GFP in nonpeptidergic nociceptors (Zylka et al., 2005; Zheng et al., 2019). mRNA transcript for Kv5.1, Kv6.2, Kv6.3, and Kv9.1 are present in GFP^{+} neurons of this mouse line (Zheng et al., 2019). We confirmed the presence of Kv5.1 and Kv9.1 transcripts in GFP^{+} neurons from *Mrgprd*^{GFP} mice (Fig 7 Supplement 1). We investigated whether these neurons have KvS-like conductances by performing whole cell voltage clamp on cultured DRG neurons that had obvious GFP fluorescence, and were bathed in the same cocktail of channel inhibitors used on SCG neurons. We found that 1 µM RY785 inhibited some current, and subsequent addition of 100 nM GxTX inhibited more current (Fig 7 A and B left panels). We analyzed tail currents identically to our analysis in SCG neurons. Tail currents from neurons after application of 1 µM RY785 were decreased by 29 $\pm$ 3% of their original amplitude (mean $\pm$ SEM) (Fig 7 B left panel, n = 7 neurons, N = 4 mice $p = 0.01$). Subsequent application of 100 nM GxTX decreased tail currents by 68 $\pm$ 5% (mean $\pm$ SEM) of their original amplitude (n = 7 neurons, N = 4 mice, $p < 0.001$). We observed no significant effect when replacing RY785 with a vehicle control in blinded,

interleaved experiments despite some current run-up and run-down (Fig 7 B right panel, n = 6 neurons, N = 4 mice). RY785 significantly decreased tail currents relative to vehicle controls (Fig 7 B p = 0.02). Concurrent application of 100 nM GxTX and 1 µM RY785 to neurons in vehicle decreased currents by 69 ± 5% (mean ± SEM) (Fig 7 B right panel, n = 6 neurons, N = 4 mice, p < 0.001). The biophysical properties of KvS-containing channels have been established for some of the KvS transcripts expressed in GFP^+ DRG neurons from *Mrgprd*^{GFP} mice. Co-expression of Kv5.1, Kv6.3 or Kv9.1 with Kv2 subunits slows deactivation of the K^+ conductance (Salinas et al., 1997a; Kramer et al., 1998; Sano et al., 2002). In Kv2.1-CHO cells transfected with Kv5.1 or Kv9.1, we confirmed that RY785-resistant currents deactivate slower than Kv2.1 controls (Fig 7 Supplement 2 A-B). To determine if the RY785- and GxTX-sensitive conductances in GFP^+ neurons from *Mrgprd*^{GFP} mice are consistent with previous reports of Kv2 or KvS channels, we examined the biophysical properties of the Kv2-like (RY785 sensitive) and KvS-like (RY785 resistant, GxTX sensitive) currents defined by subtraction (Fig 7 C). We found that KvS-like GxTX-sensitive currents deactivated slower than Kv2-like RY785-sensitive currents (Fig 7 C left panel and Fig 7 E and F). However, we note that Kv2 channel deactivation can also spontaneously slow over time (Tilley et al., 2019) and it was necessary to apply RY785 before GxTX in these studies. Kv2-like and KvS-like channel conductances began at -40 mV and had half maximal conductances around -15 mV (Fig 7 D). These results are consistent with Kv2 or KvS channels (Kramer et al., 1998; Richardson and Kaczmarek, 2000; Sano et al., 2002; Thorneloe and Nelson, 2003). Together these results indicate that in these mouse DRG neurons, RY785-sensitive currents are Kv2-like and RY785-resistant but GxTX-sensitive currents are KvS-like. Of the total conductance sensitive to RY785 and GxTX, 42 ± 3 % (mean ± SEM) was sensitive to RY785 (Kv2-like) whereas 58 ± 3 % (mean ± SEM) was resistant to RY785 but sensitive to GxTX (KvS-like) (Fig 7 G). Overall, these results show that a neuronal subtype with KvS transcripts has endogenous voltage-gated currents with KvS-like pharmacology and gating.

- Human somatosensory neurons have KvS-like conductances

Kv2-targeted drug leads have suffered from side effects due to poor tissue and cell specificity (Li et al., 2013). As KvS transcripts show far greater tissue- and cell-type specific expression relative to Kv2 (Bishop et al., 2015; Bocksteins, 2016), KvS-targeted drugs promise greater specificity. Establishing that KvS subunits form channels in humans is an important prerequisite to pursuing any KvS-targeting therapeutic strategy. We conducted experiments to determine if human DRG neurons have KvS-like conductances. Human DRG neurons express Kv2 proteins (Stewart et al., 2024), and express KvS transcripts (Ray et al., 2018) suggesting they may have KvS conductances. We performed whole-cell voltage clamp on cultured human DRG neurons, choosing smaller-diameter neurons and using the same solutions as mouse DRG neuron recordings. Any effect of 1 µM RY785 on human DRG neuron current amplitude was not distinct from interleaved vehicle controls. However, washing in 100 nM GxTX after pre-exposure to 1 µM RY785 or concurrent application of 100 nM GxTX and 1 µM RY785 dramatically inhibited currents (Fig 8 A and B, n = 3, 4 neurons, p = 0.02, 0.01 respectively, N = 1 human). The GxTX sensitivity indicates that human DRG neurons have conductances from Kv2-containing channels, and the RY785 insensitivity of GxTX-sensitive conductances suggests the underlying channels contain KvS subunits. We examined the biophysical properties of RY785- and GxTX-sensitive currents defined by subtraction (Fig 8 C). Unlike the variable vehicle subtraction currents, RY785 subtraction currents activated and deactivated with Kv2-like kinetics and were half maximal between -10 and 0 mV (Fig 8 D). The RY785-insensitive GxTX-sensitive, KvS/2-like conductances began to be apparent near -40 mV and were half maximal between -10 and 0 mV (Fig 8 D). Together these results indicate that in human DRG neurons RY785 sensitive currents are Kv2-like and that GxTX sensitive currents after application of RY785 are KvS-like. In these human DRG neurons, of the total conductance sensitive to RY785 or GxTX,

76 ± 2 % (mean ± SEM) was resistant to RY785 but sensitive to GxTX, consistent with the majority of channels containing KvS subunits (Fig 8 E). Overall, these results show human DRG neurons can have endogenous voltage-gated currents with KvS-like pharmacology and gating.

DISCUSSION

These results identify a method for pharmacologically isolating native KvS conductances. RY785 can selectively block homomeric Kv2 channels. Subsequent application of GxTX can selectively inhibit KvS conductances which are then revealed in the subtraction currents. Such a protocol could aid in identification and characterization of KvS/Kv2 conductances separately from the Kv2 homomers that are likely to be expressed in the same cell. Characterization of these now separable conductances can reveal impacts of Kv2-only channels and KvS-containing channels on electrophysiological signaling. This could be valuable as there are few tools to probe the contributions of KvS subunits to electrical signaling.

It is remarkable that resistance to RY785 is a shared property of all the KvS families. We found Kv8.1/Kv2.1 conductances to be ~1000 times less sensitive to RY785 than Kv2.1 homomer conductances in the same cell line. Based on the observation that >50% of Kv current was resistant to 1 µM RY785 in some Kv2.1-CHO cells transfected with Kv5.1, Kv6.4, or Kv9.3, these KvS/Kv2.1 channels are expected to have IC_{50} > 1 µM, or over 100-fold less sensitive than the ~10 nM IC_{50} for Kv2.1 in this cell line. This suggests that the RY785 inhibitory site is substantially disrupted by these KvS subunits. The site disruption by KvS subunits could result from steric change in the binding site itself, or could be allosteric. In Kv2.1, intracellular tetraethylammonium competes with RY785 inhibition, and voltage sensor movement gates RY785 access to its inhibitory site, suggesting that RY785 binds within the gated intracellular cavity lined by transmembrane segment S6 helices. The S6 residues lining this cavity are distinct in all KvS subunits (Marquis and Sack, 2022). The precise subunit compositions of KvS channels are debated, with evidence for Kv2:KvS stoichiometries of either 2:2 (Moller et al., 2020) or 3:1 (Kerschensteiner et al., 2005; Pisupati et al., 2018). If KvS subunits sterically disrupt the RY785 site, this would suggest that the RY785 site spans multiple Kv2 subunits, at least one of which is replaced in the KvS/Kv2 heteromers. If the KvS disruption of RY785 inhibition is allosteric, KvS subunits reduce the occurrence of channel state(s) which bind most tightly to RY785. Allosteric interactions between RY785 inhibition and channel gating are apparent for Kv2.1: inhibition kinetics of RY785 are voltage-dependent and RY785 alters voltage-sensor movements, indicating that RY785 affinity must be state-dependent (Marquis and Sack, 2022). We note that the altered Kv8.1/Kv2.1 conductance kinetics in 35 µM RY785 are consistent with state-dependent binding (Fig. 3). An allosteric mechanism seems generally plausible, as all KvS subunits imbue kinetics and voltage dependencies distinct from Kv2 (Bocksteins, 2016). For example, Kv6.4 alters the voltage-dependence of Kv2.1 subunits (Bocksteins et al., 2017), and alters dynamics of the S6 pore-gating apparatus (Pisupati et al., 2018). Notably, the S6 helical bundle crossing of Kv2.1 constricts asymmetrically during channel inactivation in ways that are allosterically modulated by 4-aminopyridine (Fernández-Mariño et al., 2023), and KvS channels allosterically alter interactions with 4-aminopyridine (Stas et al., 2015). These observations make it seem likely that KvS subunits could allosterically disrupt RY785 inhibition.

While we have identified a potential means to isolate KvS conductances, it is important to consider the limitations of these findings.

First, although every KvS subunit we tested is resistant to RY785, and these subunits span all the KvS subfamilies (Kv5, Kv6, Kv8, and Kv9), we have not tested all KvS subunits, species variants, cell types, or voltage regimens. Any of these could alter the RY785 IC_{50}. Pharmacology can yield surprises, such as the unexpected resistance of human Nav1.7 to saxitoxin (Walker et al., 2012). The degree of resistance

to RY785 may vary among KvS subunits considering this is likely with other central cavity drugs such as tetraethylammonium and 4-aminopyridine (Post et al., 1996; Thorneloe and Nelson, 2003; Stas et al., 2015). While Kv8.1/Kv2.1 channels appeared to be homogenously susceptible to RY785 (with Hill slope close to 1), other KvS subunits might present multiple pharmacologically-distinct heteromer populations.

Second, it is possible that RY785 may modulate other voltage gated channels. However, we think RY785 is unlikely to have substantial off-target effects as RY785 is much less potent against other non-Kv2 voltage gated potassium channel subtypes as well as voltage gated sodium and calcium channels (Herrington et al., 2011).

Third, concentrations of RY785 which partially blocked Kv8.1/Kv2.1 modified the gating of the voltage-activated conductance, indicating that RY785 can create a conductance with novel kinetics, or potentially even a gain-of-function under certain conditions. Notably, 4-aminopyridine can increase Kv2 or KvS conductance under specialized conditions (Stas et al., 2015). As discussed above, channel state-dependent binding is expected to influence the affinity of RY785.

Fourth, it is possible that other factors could imbue RY785 resistance. While it seems unlikely that non-KvS pore-forming Kv subunits will be found to complex with Kv2 subunits, other factors could potentially disrupt the RY785 site. Modified residues within the Kv2.1 pore might possibly prevent RY785 binding. Extensive homeostatic regulation of Kv2.1 gating maintains neuronal excitability (Misonou et al., 2006). Regulation of the gating of Kv2 channels could potentially allosterically disrupt RY785 inhibition. Ischemia (Misonou et al., 2005; Aras et al., 2009), glutamate (Misonou et al., 2008), phosphorylation (Murakoshi et al., 1997) and SUMOylation (Plant et al., 2011) and AMIGO auxiliary subunits (Peltola et al., 2011; Maverick et al., 2021) all alter Kv2 gating.

Despite all these possibilities, we think the most parsimonious interpretation of RY785-resistant, GxTX-sensitive conductances is that they are produced by KvS/Kv2 channels. However, it is important to consider the above possibilities, and perhaps others, when interpreting RY785 resistance of GxTX-sensitive conductances. With this is mind, we suggest that RY785-resistance combined with GxTX-sensitivity is strong evidence for KvS/Kv2 channels.

Delayed-rectifier Kv2-like conductances are prominent in many electrically excitable cell types. Our findings in *Mrgprd*-lineage mouse DRG as well as human DRG neurons suggest that the majority of the Kv2 conductance originates from KvS/Kv2 channels, while in mouse SCG neurons Kv2-only channels seem to predominate. Beyond these cell types, it is unclear how prevalent KvS conductances are. While Kv2 subunits are broadly expressed in electrically-excitable cells throughout the brain and body, each KvS transcript has more restricted expression pattern (Bocksteins, 2016), and these can fluctuate with age (Regnier et al., 2016). However, transcript levels alone are not sufficient to predict protein levels (Liu et al., 2016). Previous studies have used knockout mice (Regnier et al., 2017; Miyamae et al., 2021), transient transfection of KvS subunits (Lee et al., 2020), siRNA knockdown (Tsantoulas et al., 2012), and modeling (Miyamae et al., 2021) to probe the presence of endogenous and functional KvS channels, and these methods can identify phenotypic changes and suggest potential roles of KvS channels. Solid evidence for KvS proteins has been more scant, raising the question of just how common KvS/Kv2 channels are.

Recently, we found that native Kv2 channels in brain commonly contain KvS subunits, with Kv5.1 being the most abundant. Kv5.1 immunoprecipitation from mouse brain lysates retrieved 16% of the total Kv2.1 proteins indicating that a substantial fraction of Kv2 channels are Kv5.1/Kv2 heteromers (Ferns et al., 2024). This raises the possibility that many native Kv2 channels in brain are actually KvS/Kv2. Yet there is little evidence for functional KvS subunits in central neurons. The unique pharmacology of KvS-containing channels identified here provides a new and direct method of identifying KvS-like conductances, and establishing what contributions KvS subunits make to electrophysiological signaling.

REFERENCES

Aras MA, Saadi RA, Aizenman E (2009) Zn2+ regulates Kv2.1 voltage-dependent gating and localization following ischemia. Eur J Neurosci 30:2250-2257.

Bishop HI, Guan D, Bocksteins E, Parajuli LK, Murray KD, Cobb MM, Misonou H, Zito K, Foehring RC, Trimmer JS (2015) Distinct cell- and layer-specific expression patterns and independent regulation of Kv2 channel subtypes in cortical pyramidal neurons. J Neurosci 35:14922-14942.

Bocksteins E (2016) Kv5, Kv6, Kv8, and Kv9 subunits: No simple silent bystanders. J Gen Physiol 147:105-125.

Bocksteins E, Snyders DJ (2012) Electrically silent Kv subunits: their molecular and functional characteristics. Physiology (Bethesda) 27:73-84.

Bocksteins E, Snyders DJ, Holmgren M (2017) Independent movement of the voltage sensors in K(V)2.1/K(V)6.4 heterotetramers. Sci Rep 7:41646.

Bocksteins E, Labro AJ, Snyders DJ, Mohapatra DP (2012) The electrically silent Kv6.4 subunit confers hyperpolarized gating charge movement in Kv2.1/Kv6.4 heterotetrameric channels. PLoS One 7:e37143.

Bocksteins E, Raes AL, Van de Vijver G, Bruyns T, Van Bogaert PP, Snyders DJ (2009) Kv2.1 and silent Kv subunits underlie the delayed rectifier K+ current in cultured small mouse DRG neurons. Am J Physiol Cell Physiol 296:C1271-1278.

Castellano A, Chiara MD, Mellstrom B, Molina A, Monje F, Naranjo JR, Lopez-Barneo J (1997) Identification and functional characterization of a K+ channel alpha-subunit with regulatory properties specific to brain. J Neurosci 17:4652-4661.

Fernández-Mariño AI, Tan XF, Bae C, Huffer K, Jiang J, Swartz KJ (2023) Inactivation of the Kv2.1 channel through electromechanical coupling. Nature 622:410-417.

Ferns M, Van der List D, Vierra NC, Lacey T, Murray KD, Kirmiz M, Stewart RG, Sack JT, Trimmer JS (2024) Electrically silent KvS subunits associate with native Kv2 channels in brain and impact diverse properties of channel function. bioRxiv:2024.2001.2025.577135.

Guan D, Tkatch T, Surmeier DJ, Armstrong WE, Foehring RC (2007) Kv2 subunits underlie slowly inactivating potassium current in rat neocortical pyramidal neurons. J Physiol 581:941-960.

Hart NS, Mountford JK, Voigt V, Fuller-Carter P, Barth M, Nerbonne JM, Hunt DM, Carvalho LS (2019) The Role of the Voltage-Gated Potassium Channel Proteins Kv8.2 and Kv2.1 in Vision and Retinal Disease: Insights from the Study of Mouse Gene Knock-Out Mutations. eNeuro 6.

Herrington J, Solly K, Ratliff KS, Li N, Zhou YP, Howard A, Kiss L, Garcia ML, McManus OB, Deng Q, Desai R, Xiong Y, Kaczorowski GJ (2011) Identification of novel and selective Kv2 channel inhibitors. Mol Pharmacol 80:959-964.

Herrington J et al. (2006) Blockers of the delayed-rectifier potassium current in pancreatic beta-cells enhance glucose-dependent insulin secretion. Diabetes 55:1034-1042.

Inamdar SM, Lankford CK, Poria D, Laird JG, Solessio E, Kefalov VJ, Baker SA (2022) Differential impact of Kv8.2 loss on rod and cone signaling and degeneration. Hum Mol Genet 31:1035-1050.

Jorge BS, Campbell CM, Miller AR, Rutter ED, Gurnett CA, Vanoye CG, George AL, Jr., Kearney JA (2011) Voltage-gated potassium channel KCNV2 (Kv8.2) contributes to epilepsy susceptibility. Proc Natl Acad Sci U S A 108:5443-5448.

Kerschensteiner D, Stocker M (1999) Heteromeric assembly of Kv2.1 with Kv9.3: effect on the state dependence of inactivation. Biophys J 77:248-257.

Kerschensteiner D, Soto F, Stocker M (2005) Fluorescence measurements reveal stoichiometry of K+ channels formed by modulatory and delayed rectifier alpha-subunits. Proc Natl Acad Sci U S A 102:6160-6165.

Kihira Y, Hermanstyne TO, Misonou H (2010) Formation of heteromeric Kv2 channels in mammalian brain neurons. J Biol Chem 285:15048-15055.
Kirmiz M, Palacio S, Thapa P, King AN, Sack JT, Trimmer JS (2018) Remodeling neuronal ER-PM junctions is a conserved nonconducting function of Kv2 plasma membrane ion channels. Mol Biol Cell:mbcE18050337.
Kobertz WR (2018) Oddballs in the Shaker family: Kv2-related regulatory subunits. J Gen Physiol 150:1599-1601.
Kramer JW, Post MA, Brown AM, Kirsch GE (1998) Modulation of potassium channel gating by coexpression of Kv2.1 with regulatory Kv5.1 or Kv6.1 alpha-subunits. Am J Physiol 274:C1501-1510.
Lee MC, Nahorski MS, Hockley JRF, Lu VB, Ison G, Pattison LA, Callejo G, Stouffer K, Fletcher E, Brown C, Drissi I, Wheeler D, Ernfors P, Menon D, Reimann F, Smith ESJ, Woods CG (2020) Human labor pain is influenced by the voltage-gated potassium channel Kv 6.4 subunit. Cell Rep 32:107941.
Li XN, Herrington J, Petrov A, Ge L, Eiermann G, Xiong Y, Jensen MV, Hohmeier HE, Newgard CB, Garcia ML, Wagner M, Zhang BB, Thornberry NA, Howard AD, Kaczorowski GJ, Zhou YP (2013) The role of voltage-gated potassium channels Kv2.1 and Kv2.2 in the regulation of insulin and somatostatin release from pancreatic islets. J Pharmacol Exp Ther 344:407-416.
Liu PW, Bean BP (2014) Kv2 channel regulation of action potential repolarization and firing patterns in superior cervical ganglion neurons and hippocampal CA1 pyramidal neurons. J Neurosci 34:4991-5002.
Liu Y, Beyer A, Aebersold R (2016) On the Dependency of Cellular Protein Levels on mRNA Abundance. Cell 165:535-550.
Marquis MJ, Sack JT (2022) Mechanism of use-dependent Kv2 channel inhibition by RY785. J Gen Physiol 154.
Matsumoto C, O'Dwyer SC, Manning D, Hernandez-Hernandez G, Rhana P, Fong Z, Sato D, Clancy CE, Vierra NC, Trimmer JS, Fernando Santana L (2023) The formation of K(V)2.1 macro-clusters is required for sex-specific differences in L-type Ca(V)1.2 clustering and function in arterial myocytes. Commun Biol 6:1165.
Maverick EE, Leek AN, Tamkun MM (2021) Kv2 channel-AMIGO β-subunit assembly modulates both channel function and cell adhesion molecule surface trafficking. J Cell Sci 134.
Milescu M, Lee HC, Bae CH, Kim JI, Swartz KJ (2013) Opening the shaker K+ channel with hanatoxin. J Gen Physiol 141:203-216.
Milescu M, Bosmans F, Lee S, Alabi AA, Kim JI, Swartz KJ (2009) Interactions between lipids and voltage sensor paddles detected with tarantula toxins. Nat Struct Mol Biol 16:1080-1085.
Misonou H, Thompson SM, Cai X (2008) Dynamic regulation of the Kv2.1 voltage-gated potassium channel during brain ischemia through neuroglial interaction. J Neurosci 28:8529-8538.
Misonou H, Mohapatra DP, Menegola M, Trimmer JS (2005) Calcium- and metabolic state-dependent modulation of the voltage-dependent Kv2.1 channel regulates neuronal excitability in response to ischemia. J Neurosci 25:11184-11193.
Misonou H, Menegola M, Mohapatra DP, Guy LK, Park KS, Trimmer JS (2006) Bidirectional activity-dependent regulation of neuronal ion channel phosphorylation. J Neurosci 26:13505-13514.
Miyamae T, Hashimoto T, Abraham M, Kawabata R, Koshikizawa S, Bian Y, Nishihata Y, Kikuchi M, Ermentrout GB, Lewis DA, Gonzalez-Burgos G (2021) Kcns3 deficiency disrupts Parvalbumin neuron physiology in mouse prefrontal cortex: Implications for the pathophysiology of schizophrenia. Neurobiol Dis 155:105382.
Moller L, Regnier G, Labro AJ, Blunck R, Snyders DJ (2020) Determining the correct stoichiometry of Kv2.1/Kv6.4 heterotetramers, functional in multiple stoichiometrical configurations. Proc Natl Acad Sci U S A 117:9365-9376.

Murakoshi H, Shi G, Scannevin RH, Trimmer JS (1997) Phosphorylation of the Kv2.1 K+ channel alters voltage-dependent activation. Mol Pharmacol 52:821-828.
Peltola MA, Kuja-Panula J, Lauri SE, Taira T, Rauvala H (2011) AMIGO is an auxiliary subunit of the Kv2.1 potassium channel. EMBO Rep 12:1293-1299.
Pisupati A, Mickolajczyk KJ, Horton W, van Rossum DB, Anishkin A, Chintapalli SV, Li X, Chu-Luo J, Busey G, Hancock WO, Jegla T (2018) The S6 gate in regulatory Kv6 subunits restricts heteromeric K. J Gen Physiol 150:1702-1721.
Plant LD, Dowdell EJ, Dementieva IS, Marks JD, Goldstein SA (2011) SUMO modification of cell surface Kv2.1 potassium channels regulates the activity of rat hippocampal neurons. J Gen Physiol 137:441-454.
Post MA, Kirsch GE, Brown AM (1996) Kv2.1 and electrically silent Kv6.1 potassium channel subunits combine and express a novel current. FEBS Lett 399:177-182.
Ray P, Torck A, Quigley L, Wangzhou A, Neiman M, Rao C, Lam T, Kim JY, Kim TH, Zhang MQ, Dussor G, Price TJ (2018) Comparative transcriptome profiling of the human and mouse dorsal root ganglia: an RNA-seq-based resource for pain and sensory neuroscience research. Pain 159:1325-1345.
Regnier G, Bocksteins E, Van de Vijver G, Snyders DJ, van Bogaert PP (2016) The contribution of Kv2.2-mediated currents decreases during the postnatal development of mouse dorsal root ganglion neurons. Physiol Rep 4.
Regnier G, Bocksteins E, Marei WF, Pintelon I, Timmermans JP, Leroy JLMR, Snyders DJ (2017) Targeted deletion of the Kv6.4 subunit causes male sterility due to disturbed spermiogenesis. Reprod Fertil Dev 29:1567-1575.
Richardson FC, Kaczmarek LK (2000) Modification of delayed rectifier potassium currents by the Kv9.1 potassium channel subunit. Hear Res 147:21-30.
Salinas M, Duprat F, Heurteaux C, Hugnot JP, Lazdunski M (1997a) New modulatory alpha subunits for mammalian Shab K+ channels. The Journal of biological chemistry 272:24371-24379.
Salinas M, de Weille J, Guillemare E, Lazdunski M, Hugnot JP (1997b) Modes of regulation of shab K+ channel activity by the Kv8.1 subunit. J Biol Chem 272:8774-8780.
Sano Y, Mochizuki S, Miyake A, Kitada C, Inamura K, Yokoi H, Nozawa K, Matsushime H, Furuichi K (2002) Molecular cloning and characterization of Kv6.3, a novel modulatory subunit for voltage-gated K(+) channel Kv2.1. FEBS Lett 512:230-234.
Sapio MR, Vazquez FA, Loydpierson AJ, Maric D, Kim JJ, LaPaglia DM, Puhl HL, Lu VB, Ikeda SR, Mannes AJ, Iadarola MJ (2020) Comparative Analysis of Dorsal Root, Nodose and Sympathetic Ganglia for the Development of New Analgesics. Front Neurosci 14:615362.
Sepela RJ, Stewart RG, Valencia LA, Thapa P, Wang Z, Cohen BE, Sack JT (2022) The AMIGO1 adhesion protein activates Kv2.1 voltage sensors. Biophys J 121:1395-1416.
Speca DJ, Ogata G, Mandikian D, Bishop HI, Wiler SW, Eum K, Wenzel HJ, Doisy ET, Matt L, Campi KL, Golub MS, Nerbonne JM, Hell JW, Trainor BC, Sack JT, Schwartzkroin PA, Trimmer JS (2014) Deletion of the Kv2.1 delayed rectifier potassium channel leads to neuronal and behavioral hyperexcitability. Genes Brain Behav 13:394-408.
Stas JI, Bocksteins E, Labro AJ, Snyders DJ (2015) Modulation of Closed-State Inactivation in Kv2.1/Kv6.4 Heterotetramers as Mechanism for 4-AP Induced Potentiation. PLoS One 10:e0141349.
Stewart RG, Camacena M, Copits BA, Sack JT (2024) Distinct cellular expression and subcellular localization of Kv2 voltage-gated K(+) channel subtypes in dorsal root ganglion neurons conserved between mice and humans. In: *Journal of Comparative Neurology accepted, in press* PMID: 38187582; PMC10769185.

Thapa P, Stewart R, Sepela RJ, Vivas O, Parajuli LK, Lillya M, Fletcher-Taylor S, Cohen BE, Zito K, Sack JT (2021) EVAP: A two-photon imaging tool to study conformational changes in endogenous Kv2 channels in live tissues. J Gen Physiol 153.

Thorneloe KS, Nelson MT (2003) Properties and molecular basis of the mouse urinary bladder voltage-gated K+ current. J Physiol 549:65-74.

Tilley DC, Angueyra JM, Eum KS, Kim H, Chao LH, Peng AW, Sack JT (2019) The tarantula toxin GxTx detains K. J Gen Physiol 151:292-315.

Tilley DC, Eum KS, Fletcher-Taylor S, Austin DC, Dupré C, Patrón LA, Garcia RL, Lam K, Yarov-Yarovoy V, Cohen BE, Sack JT (2014) Chemoselective tarantula toxins report voltage activation of wild-type ion channels in live cells. Proceedings of the National Academy of Sciences of the United States of America 111:E4789-E4796.

Tsantoulas C, Denk F, Signore M, Nassar MA, Futai K, McMahon SB (2018) Mice lacking Kcns1 in peripheral neurons show increased basal and neuropathic pain sensitivity. Pain 159:1641-1651.

Tsantoulas C, Zhu L, Shaifta Y, Grist J, Ward JP, Raouf R, Michael GJ, McMahon SB (2012) Sensory neuron downregulation of the Kv9.1 potassium channel subunit mediates neuropathic pain following nerve injury. J Neurosci 32:17502-17513.

Valtcheva MV, Copits BA, Davidson S, Sheahan TD, Pullen MY, McCall JG, Dikranian K, Gereau RWt (2016) Surgical extraction of human dorsal root ganglia from organ donors and preparation of primary sensory neuron cultures. Nat Protoc 11:1877-1888.

Vierra NC, O'Dwyer SC, Matsumoto C, Santana LF, Trimmer JS (2021) Regulation of neuronal excitation-transcription coupling by Kv2.1-induced clustering of somatic L-type Ca(2+) channels at ER-PM junctions. Proc Natl Acad Sci U S A 118.

Walker JR, Novick PA, Parsons WH, McGregor M, Zablocki J, Pande VS, Du Bois J (2012) Marked difference in saxitoxin and tetrodotoxin affinity for the human nociceptive voltage-gated sodium channel (Nav1.7) [corrected]. Proc Natl Acad Sci U S A 109:18102-18107.

Wu H, Cowing JA, Michaelides M, Wilkie SE, Jeffery G, Jenkins SA, Mester V, Bird AC, Robson AG, Holder GE, Moore AT, Hunt DM, Webster AR (2006) Mutations in the gene KCNV2 encoding a voltage-gated potassium channel subunit cause "cone dystrophy with supernormal rod electroretinogram" in humans. Am J Hum Genet 79:574-579.

Zheng Y, Liu P, Bai L, Trimmer JS, Bean BP, Ginty DD (2019) Deep sequencing of somatosensory neurons reveals molecular determinants of intrinsic physiological properties. Neuron 103:598-616.e597.

Zhong XZ, Abd-Elrahman KS, Liao CH, El-Yazbi AF, Walsh EJ, Walsh MP, Cole WC (2010) Stromatoxin-sensitive, heteromultimeric Kv2.1/Kv9.3 channels contribute to myogenic control of cerebral arterial diameter. J Physiol 588:4519-4537.

Zylka MJ, Rice FL, Anderson DJ (2005) Topographically distinct epidermal nociceptive circuits revealed by axonal tracers targeted to Mrgprd. Neuron 45:17-25.

FIGURES AND FIGURE LEGENDS

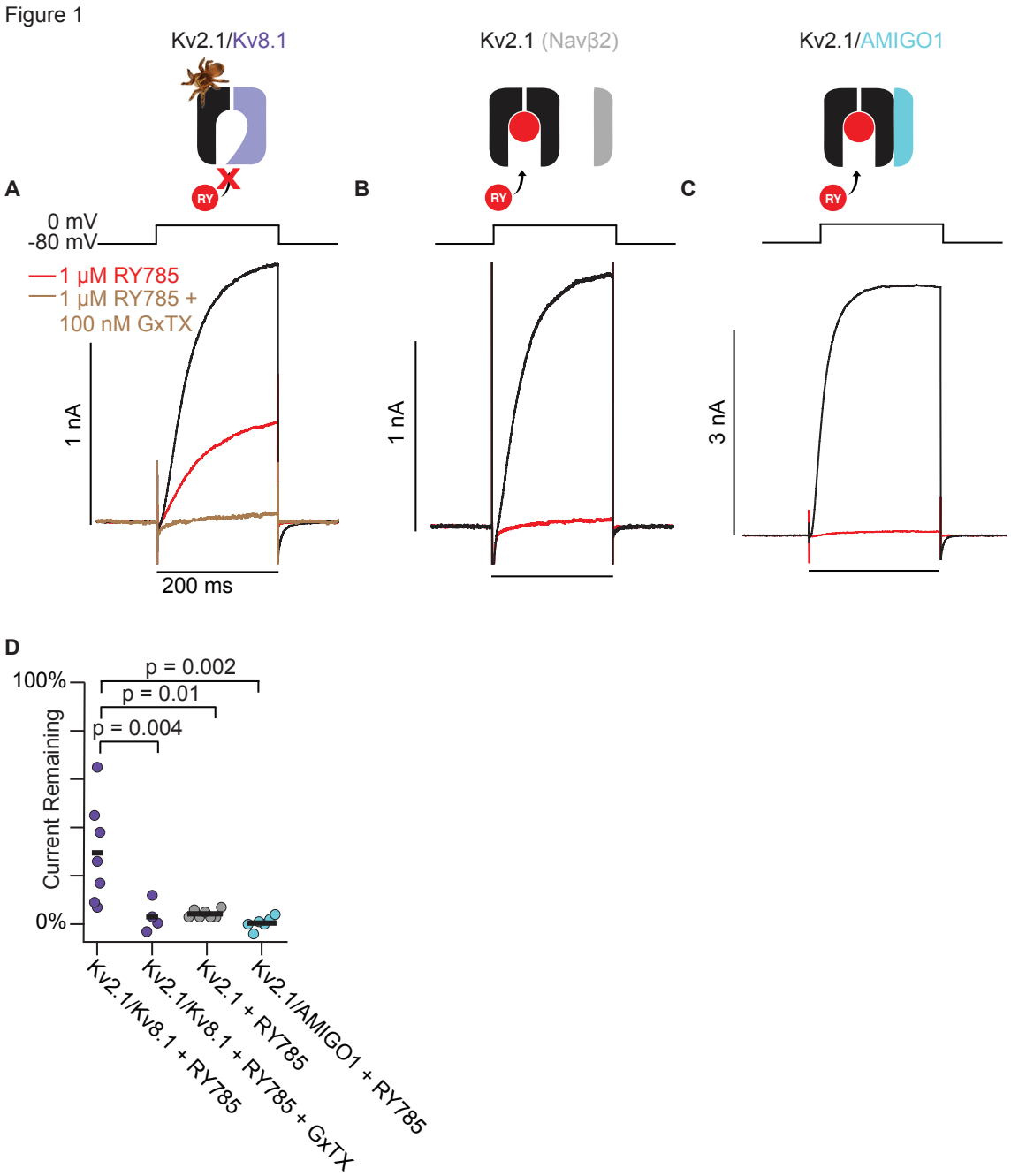

Figure 1 Kv2.1/Kv8.1 heteromers are resistant to RY785 and sensitive to GxTX

A) Exemplar traces from a Kv2.1-CHO cell transfected with Kv8.1. Black and red traces are currents before and after application of 1 uM RY785 respectively. Brown trace is current after application of 1 μM RY785 + 100 nM GxTX.
B) Exemplar traces from a Kv2.1-CHO cell transfected with Navβ2.
C) Exemplar traces from a Kv2.1-CHO cell transfected with AMIGO1.

D) Current remaining after application of 1 µM RY785 or 1 µM RY785 + 100 nM GxTX. Black bars represent mean. Each point represents current from one cell at the end of a 200 ms 0 mV voltage step. One-way ANOVA $p < 0.001$. p values in figure represent post hoc Tukey's test.

Figure 2

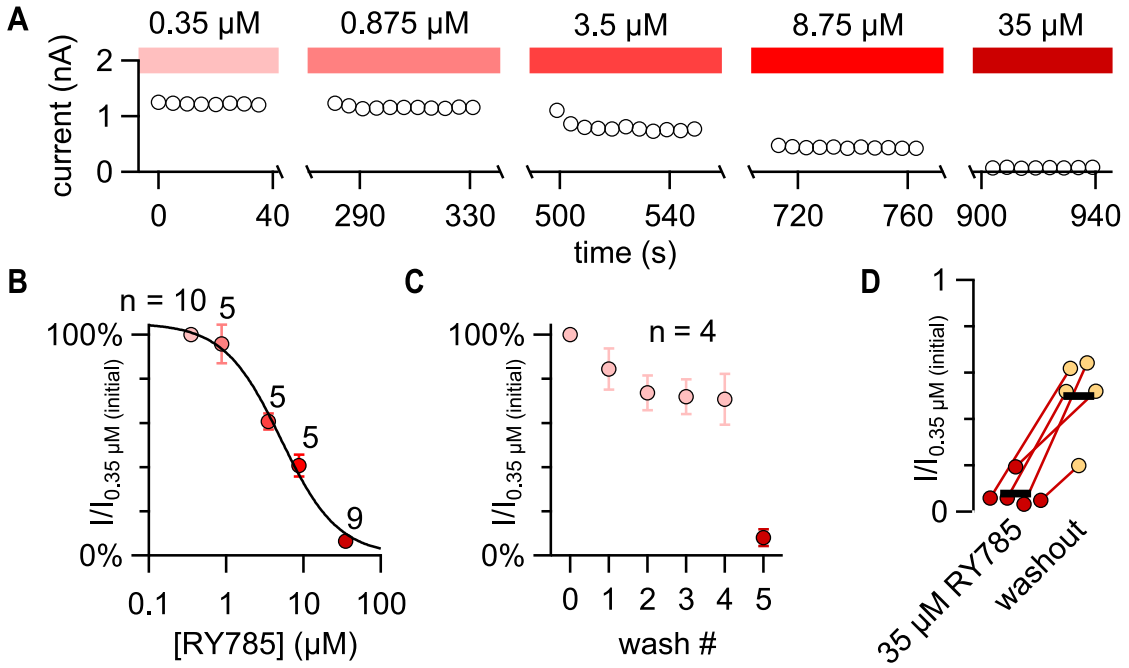

Figure 2 RY785 blocks Kv2.1/Kv8.1 heteromers in a concentration-dependent manner.

A) Representative time course of block by varying concentrations of RY785 in a Kv2.1-CHO cell transfected with Kv8.1. Symbols represent tail current amplitudes measured 2-4 ms into a step to 0 mV following a 200 ms step to 80 mV. This voltage protocol was performed once every 5 s. Darker coloring indicates a higher concentration of RY785. Solution exchanges occurred during the gaps in the time axis.
B) Mean normalized tail current amplitudes at varying concentrations of RY785. Lesser concentrations were always applied before greater concentrations. Error bars represent SEMs. Black curve is a fitted Hill function with n_H held equal to 1 (base = 1.0 ± 0.1 % IC_{50} = 5.1 ± 1.0 μM).
C) Response of voltage-gated outward current to repeated washing with 0.35 μM RY785 and one wash with 35 μM RY785 (wash #5). Error bars represent SEMs.
D) Partial wash out of 35 μM RY785 with 0.35 μM RY785. Black bars represent mean current amplitudes from N = 5 cells.

Figure 3

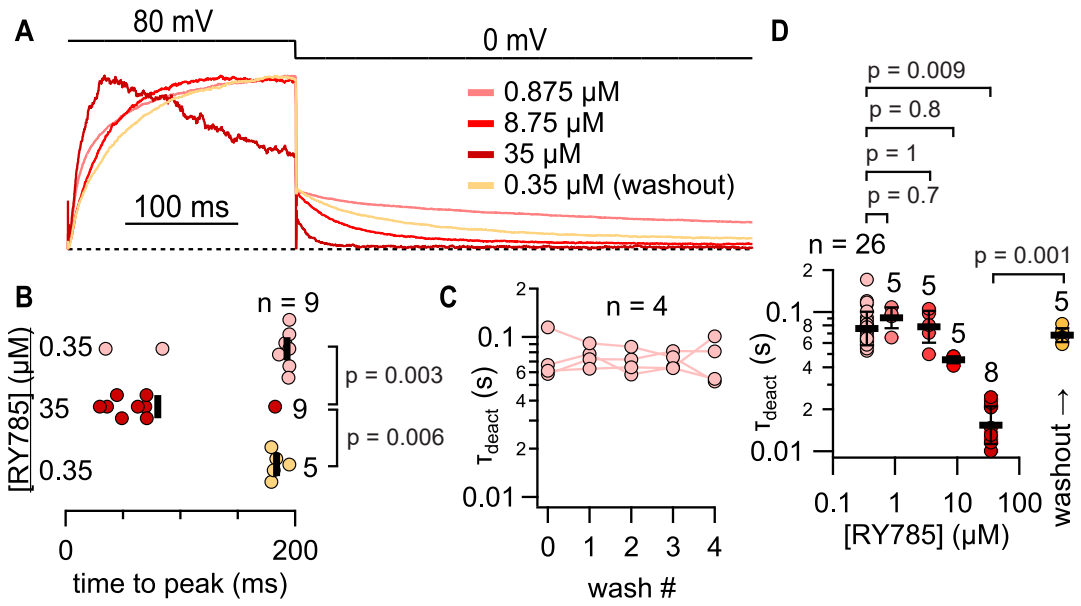

Figure 3 Increasing [RY785] affects Kv2.1/Kv8.1 channel properties.

A) Exemplar current traces in response to the indicated voltage protocol from a Kv2.1-CHO cell transfected with Kv8.1 in the presence of 0.875, 8.75, and 35 µM RY785. Traces are normalized to their maxima to illustrate modulation of gating kinetics by increasing concentrations of RY785.
B) Latency to peak current during steps to +80 mV. Cells were initially bathed in 0.35 µM RY785, then in 35 µM RY785, and finally in 0.35 µM RY785 again. Symbols connected with lines represent latencies from distinct cells. Black bars represent means. 0.35 µM RY785 (initial) vs 35 µM RY785: Two-tailed unpaired Wilcoxon rank test p = 0.003. 35 µM RY785 vs washout: one-tailed unpaired Wilcoxon rank test p = 0.006.
C) Response of voltage-gated outward current to repeated washing with 0.35 µM RY785. ANOVA p = 0.99.
D) Time constants of deactivation at 0 mV in varying concentrations of RY785. Time constants are derived from fits of Equation 3 to tail currents like those shown in Panel A. Fits were from the peak of each tail current to 200 ms after the voltage step and had A_2 set equal to 0. Unpaired Welch test p = $5x10^{-8}$. Two-tailed Dunnett tests vs 0.35 µM RY785 (initial): 0.875 µM RY785 p = 0.7, 3.5 µM RY785 p = 1, 8.75 µM RY785 p = 0.8, 35 µM RY785 p = 0.009. 35 µM RY785 vs 0.35 µM RY785 (washout): two-tailed unpaired Wilcoxon rank test p = 0.001.

Figure 4

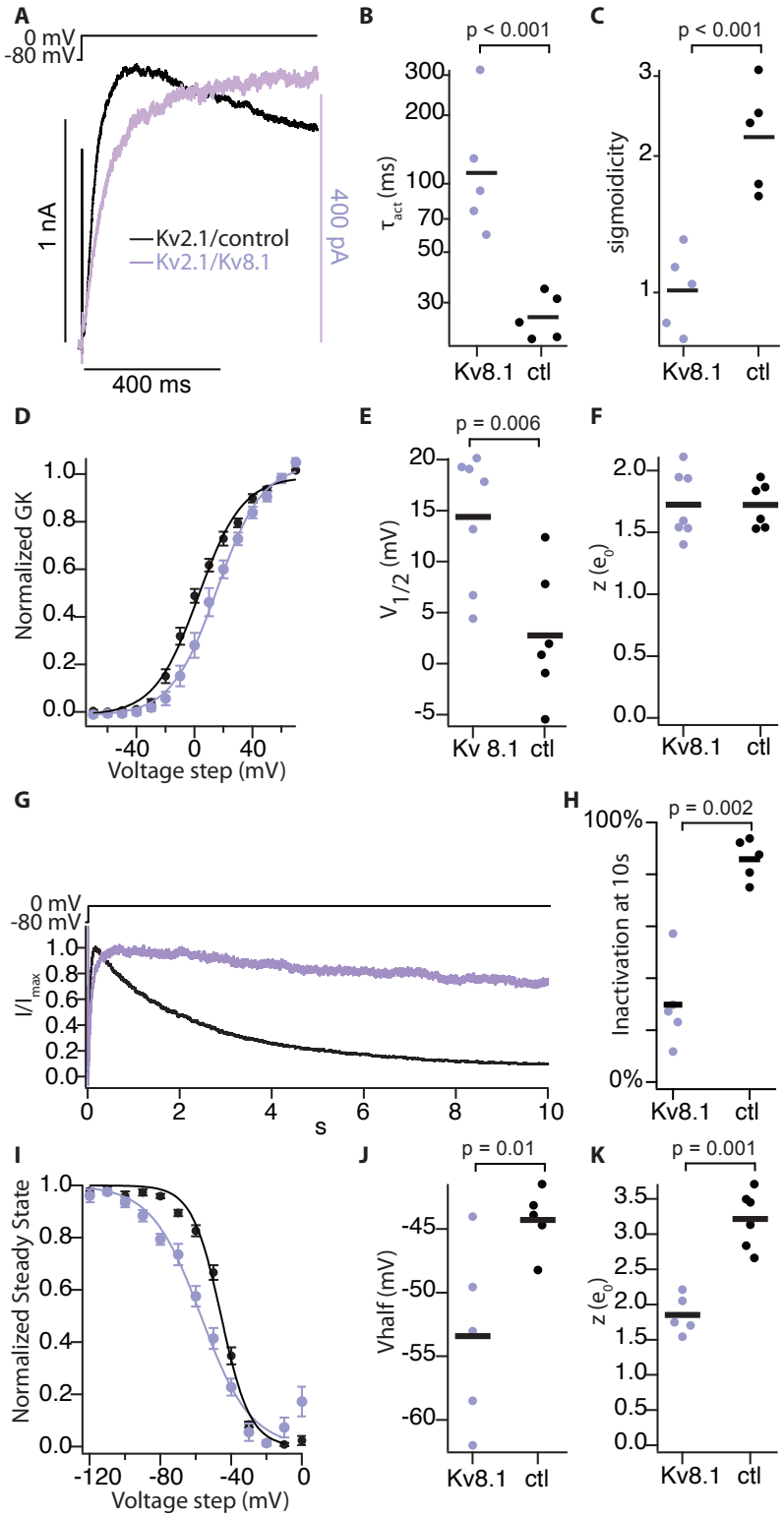

Figure 4 RY785-resistant current is consistent with Kv2.1/Kv8.1 heteromers

Kv2.1-CHO cells were transfected with Kv8.1, washed in 1 µM RY785 and given voltage steps to 0 mV until currents stabilized before measurements. Kv2.1/control are Kv2.1-CHO cells treated identically, except they were transfected with Navβ2, and washed with a vehicle control instead of 1 µM RY785. Purple data represent Kv2.1/Kv8.1 and black data represent Kv2.1/control throughout the figure.

A) Exemplar currents during a step to 0 mV. Traces are normalized to the max current during the 0 mV voltage step.
B) Time constants from exponential fit (equation 1). Geometric mean: Wilcoxon rank test.
C) Sigmoidicity from exponential fit (equation 1). Geometric mean: Wilcoxon rank test.
D) Voltage dependance of activation normalized to max conductance. Conductance was measured from initial tail currents at 0 mV. Mean ± SEM. Kv2.1/Kv8.1 n = 7 cells Kv2.1 n = 6 cells. Purple line fit (equation 2) (Kv8.1/Kv2.1: $V_{1/2}$ = 15 ± 1 mV z = 1.6 ± 0.1 e_0). Black line fit (equation 2) (Kv2.1/control: $V_{1/2}$ = 2.7 ± 1 mV z = 1.7 ± 0.1 e_0).
E) Activation $V_{1/2}$ values from Boltzmann fit (equation 2) to individual cells: Wilcoxon rank test.
F) Activation z values from Boltzmann fits.
G) Exemplar currents during a 10 s step to 0 mV. Traces are normalized to max current.
H) Percent of current inactivated after 10 seconds at 0 mV: Wilcoxon rank test.
I) Steady state currents at 0 mV after holding at indicated voltages for 10 seconds. Normalized to the max current after subtracting currents that were maximally inhibited. Mean ± SEM. Kv2.1/Kv8.1 n = 5 cells Kv2.1 n = 5 cells. Purple line fit (equation 2) (Kv8.1/Kv2.1: $V_{1/2}$ = -57 ± 1.15 mV z = 1.8 ± 0.1 e_0). Black line fit (equation 2) (Kv2.1/control: $V_{1/2}$ = -45.7 ± 0.8 mV z = 3.1 ± 0.3 e_0).
J) Inactivation $V_{1/2}$ values from Boltzmann fits (equation 2): Wilcoxon rank test.
K) Inactivation z values from Boltzmann fits (equation 2): Wilcoxon rank test.

Figure 4 Supplement

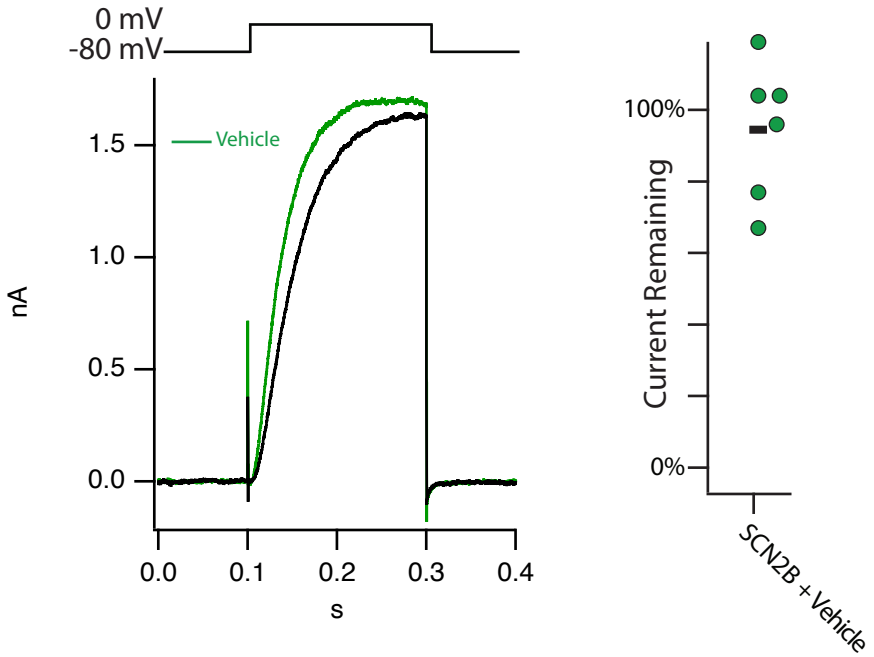

Figure 4 Supplement

Left Exemplar traces from a Kv2.1-CHO cell transfected with Navβ2. Black and green traces are currents before and after application of vehicle control respectively. Right Current remaining after application of vehicle control. Black bar represents mean. Each point represents current from one cell at the end of a 200 ms 0 mV voltage step.

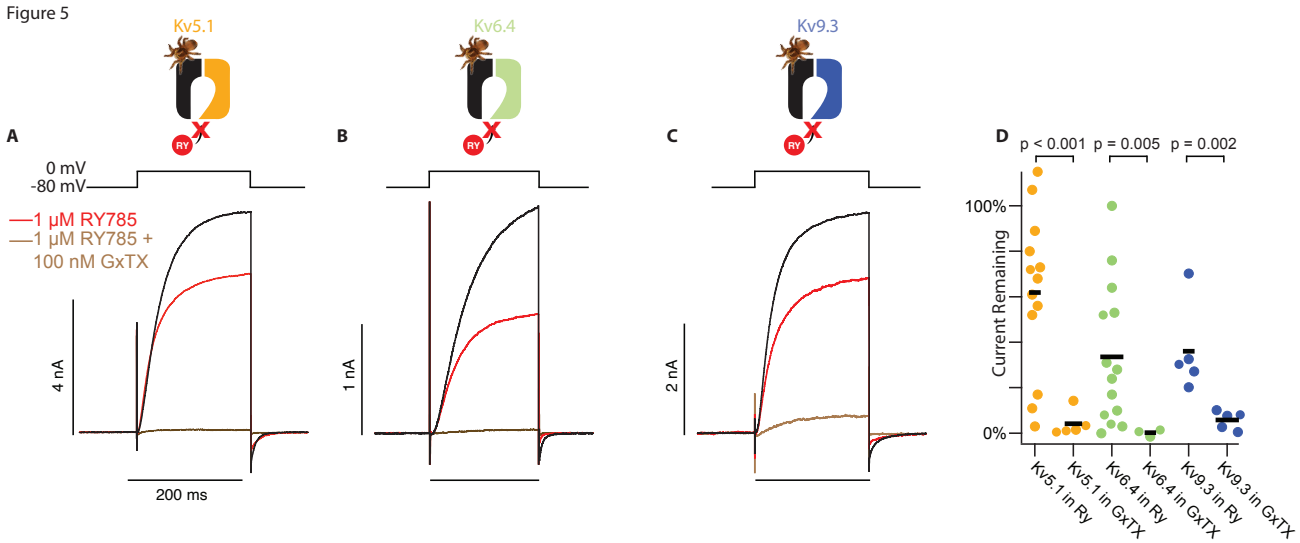

Figure 5 A subunit from each KvS family is resistant to RY785

A) Exemplar traces from a Kv2.1-CHO cell transfected with Kv5.1. Black and red traces are currents before and after application of 1 µM RY785 respectively. Brown trace is current after application of 1 µM RY785 + 100 nM GxTX.
B) Exemplar traces from a Kv2.1-CHO cell transfected with Kv6.4.
C) Exemplar traces from a Kv2.1-CHO cell transfected with Kv9.3.
D) Current remaining after application of 1 µM RY785 or 1 µM RY785 + 100 nM GxTX. Black bars represent mean. Each point represents current from one cell at the end of a 200 ms 0 mV voltage step: Wilcoxon rank test.

Figure 6

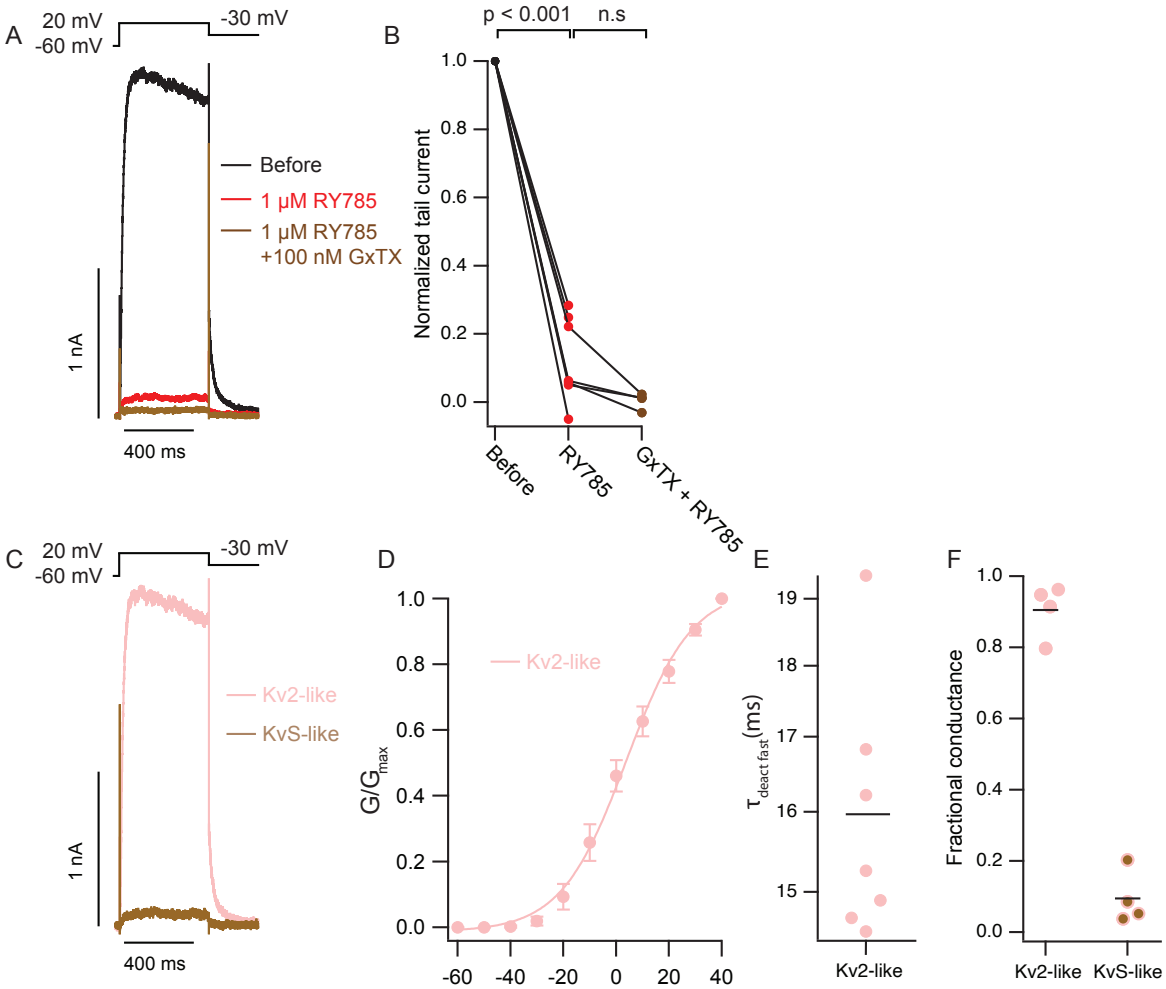

Figure 6 Mouse superior cervical ganglion (SCG) neurons have little if any RY785-resistant KvS-like currents.

A) Exemplar currents from superior cervical ganglion.
B) Tail current amplitude 10 ms after voltage was stepped from +10 mV to -40 mV normalized to current amplitude before RY785 or vehicle treatment: Wilcoxon rank test.
C) Exemplar subtracted currents from A. Kv2-like is the initial current minus in RY785 (black trace minus red in A). KvS-like is the current in RY785 minus in GxTX (red trace minus brown in A).
D) Voltage dependance of activation of Kv2-like subtraction currents in SCG neurons. Conductance was measured from initial tail currents at -40 mV. Mean ± SEM. Kv2-like n = 7 neurons N = 3 mice.
E) The faster time constant of a double exponential fit (equation 3) to channel deactivation.
F) Fractional conductance relative to the total RY785 + GxTX-sensitive conductance. Kv2-like is sensitive to RY785, KvS-like is only sensitive to GxTX.

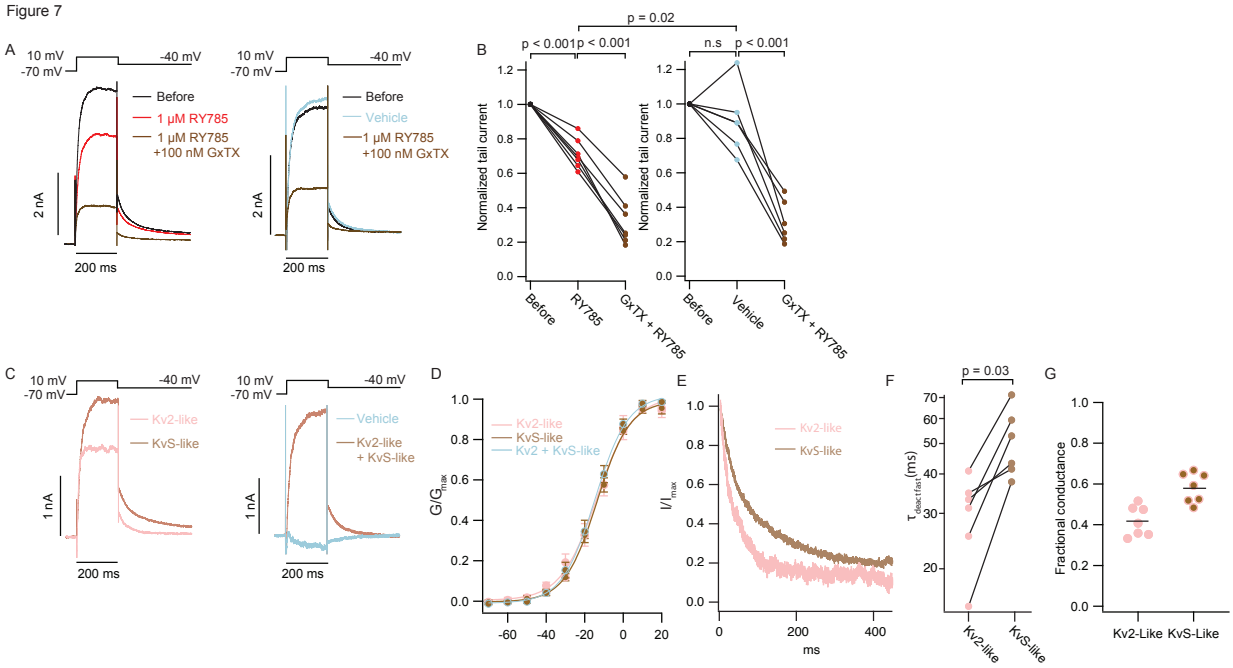

Figure 7 Mouse nociceptors have RY785-resistant KvS-like currents.

A) Exemplar currents from nonpeptidergic nociceptors.
B) Tail current amplitude 10 ms after voltage was stepped from +10 mV to -40 mV normalized to current amplitude before RY785 or vehicle treatment: Wilcoxon rank test.
C) Exemplar subtracted currents from A. Kv2-like is the initial current minus in RY785 (black trace minus red in A left panel). KvS-like is the current in RY785 minus in GxTX (red trace minus brown in A left panel). Kv2-like + KvS-like is the current in vehicle minus in RY785 + GxTX (blue trace minus brown in A right panel).
D) Voltage dependance of activation of subtraction currents in *Mrgprd*$^{GFP+}$ neurons. Pink points represent Kv2-like currents, brown points outlined with pink represent KvS like currents, and brown points outlined with light blue represent Kv2 + KvS-like currents after vehicle treatment. Conductance was measured from initial tail currents at -40 mV. Mean ± SEM. Kv2 + KvS-like n = 6 neurons N = 4 mice, KvS-like and Kv2-like n = 7 neurons N = 4 mice.
E) Ry785 (pink) and GxTX (brown) sensitive currents shown in C normalized to the max current during the -40 mV voltage step.
F) The faster time constant of a double exponential fit (equation 3) to channel deactivation: two tailed Wilcoxon signed test.
G) Fractional conductance relative to the total RY785 + GxTX-sensitive conductance. Kv2-like is sensitive to RY785, KvS-like is only sensitive to GxTX.

Figure 7 Supplement 1

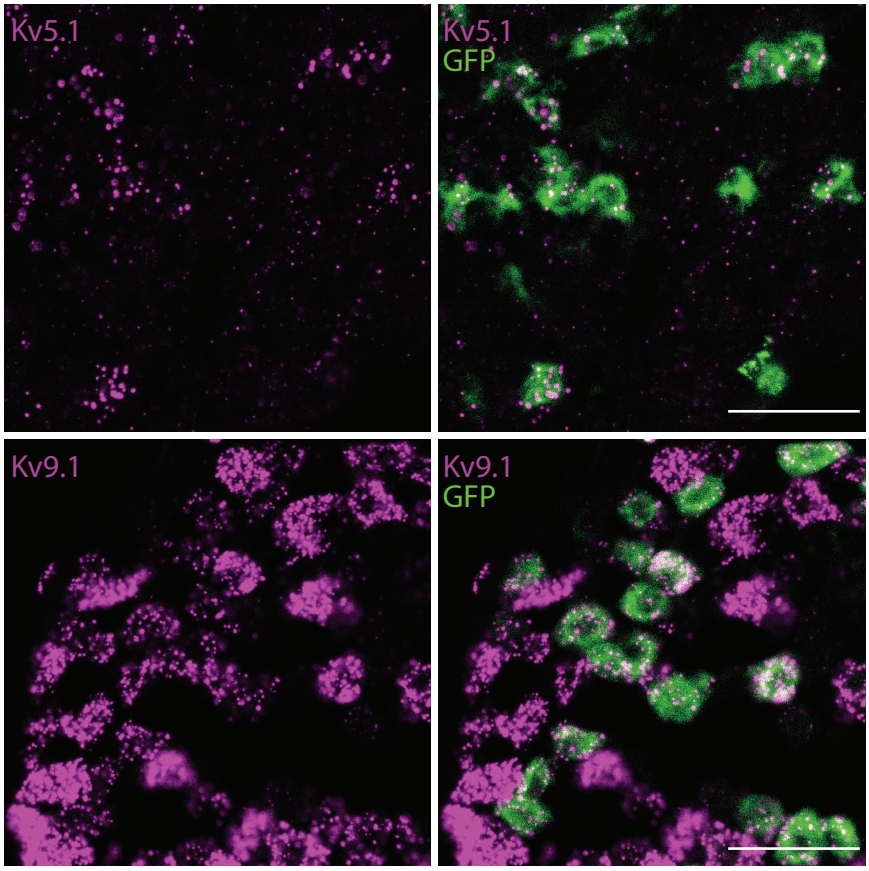

Figure 7 Supplement 1 Nonpeptidergic nociceptors express Kv5.1 and Kv9.1 mRNA transcripts

Exemplar images of DRG sections from a *Mrgprd*^{GFP} mouse labeled with RNAscope in situ hybridization for KCNF1 (Kv5.1) (top magenta) or KCNS1 (Kv9.1) (bottom magenta). Scale bars are 50 µm.

Fig 7 Supplement 2

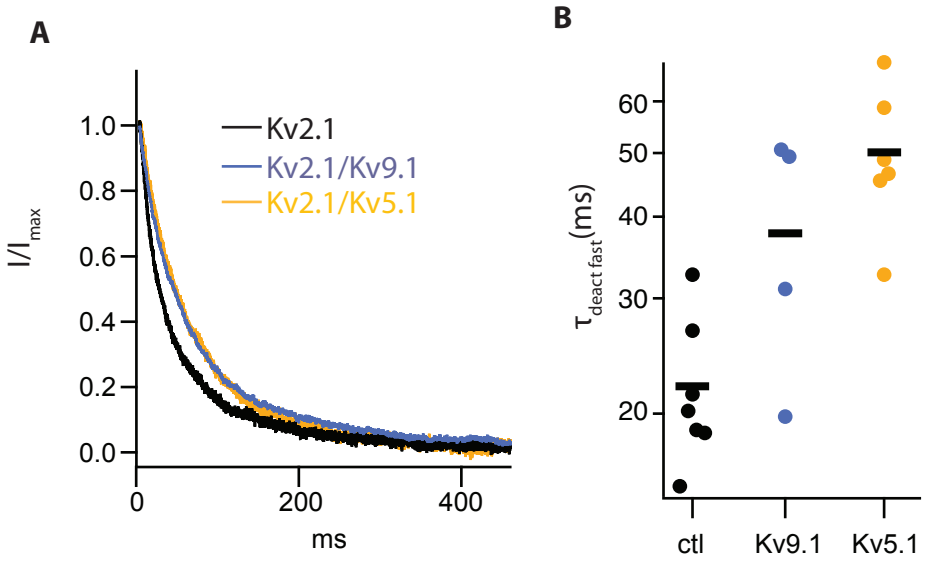

Figure 7 Supplement 2 RY785 resistant currents from Kv2.1-CHO cells transfected with Kv5.1 or Kv9.1 deactivate slower than currents from untransfected Kv2.1-CHO cell.

A) Exemplar traces of channel deactivation at -40 mV after a 50 ms step to +20 mV. Traces are normalized to max current during -40 mV step.
B) The faster time constant of a double exponential fit (equation 3) to channel deactivation.

Figure 8

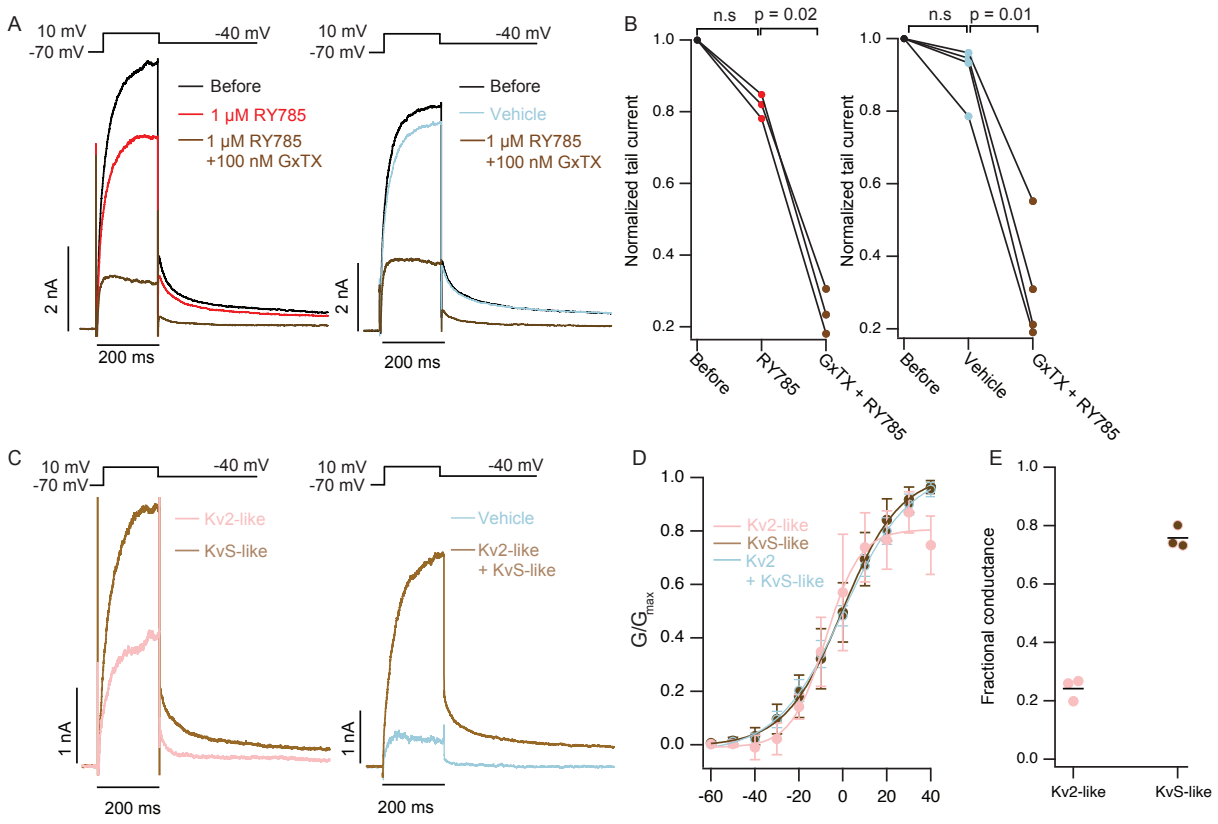

Figure 8 Human somatosensory neurons have RY785-resistant KvS-like currents.

A) Exemplar currents from human dorsal root ganglion neurons.
B) Tail current amplitude 10 ms after voltage was stepped from +10 mV to -40 mV normalized to current amplitude before RY785 or vehicle treatment: Wilcoxon rank test.
C) Exemplar subtracted currents from A. Kv2-like is the initial current minus in RY785 (black trace minus red in A left panel). KvS-like is the current in RY785 minus in GxTX (red trace minus brown in A left panel). Kv2-like + KvS-like is the current in vehicle minus in RY785 + GxTX (blue trace minus brown in A right panel).
D) Voltage dependance of activation of subtraction currents in MrgprdGFP+ neurons. Pink points represent Kv2-like currents, brown points outlined with pink represent KvS like currents, and brown points outlined with light blue represent Kv2 + KvS-like currents after vehicle treatment. Conductance was measured from initial tail currents at -40 mV. Mean ± SEM. Kv2 + KvS-like n = 3 neurons N = 1 human, KvS-like and Kv2-like n = 4 neurons N = 1 human.
E) Fractional conductance relative to the total RY785 + GxTX-sensitive conductance. Kv2-like is sensitive to RY785, KvS-like is only sensitive to GxTX.